Chapter II

Chapter II

Iridium (III) complexes – Synthesis, Characterization and computational studies

2.1. Review of Literature

Among the platinum group metal complexes, iridium (III) complexes are emerging in the field of medicinal and electronic devices because of their excellent photophysical and electrochemical properties, and in combination with heterocyclic ring systems, the properties can be more tunable and may increase their efficiency.

Mei-Jin *et al.*, have synthesised and characterized two iridium (III) complexes[1] having bipyridine as ancillary ligand. The synthesised complex exhibits highest luminescence with high quantum effects and have the potential of sensing the lectin interaction.

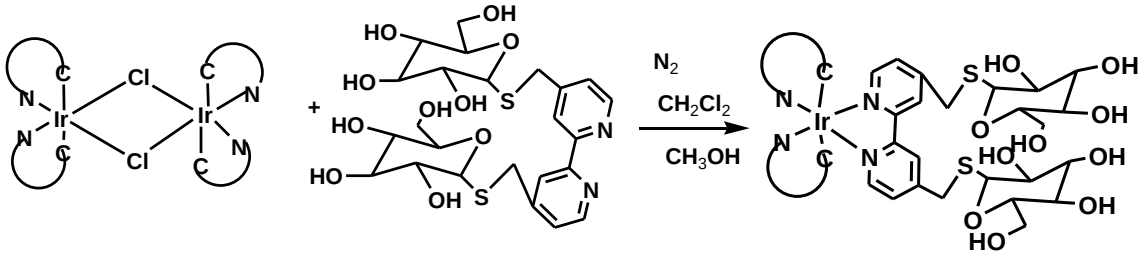

53 **54** **55**

Hajra *et al*., have synthesized and characterized the cyclometalated iridium complexes[2] containing ancillary pyrazole ligands. The photophysical and electrochemical properties of the compounds have been studied and showed the absorption / emission behavior is dependent on the $Ir(ppy)_2$ moiety of the complexes, the ancillary pyrazole ligands do not influence the photophysical behavior of the complexes.

Sivakumar reported the synthesis and photophysical characterization of Ir (III) complex[3] containing isoquinoline system. The UV spectrum revealed that the charge transfer transitions of metal to ligand were induced by interaction between singlet and triplet coupling. The PL spectra explained that increase in doping concentration decreases the PL lifetime. The efficiency of the complex exhibited in OLED device is 3007 cd/m^2.

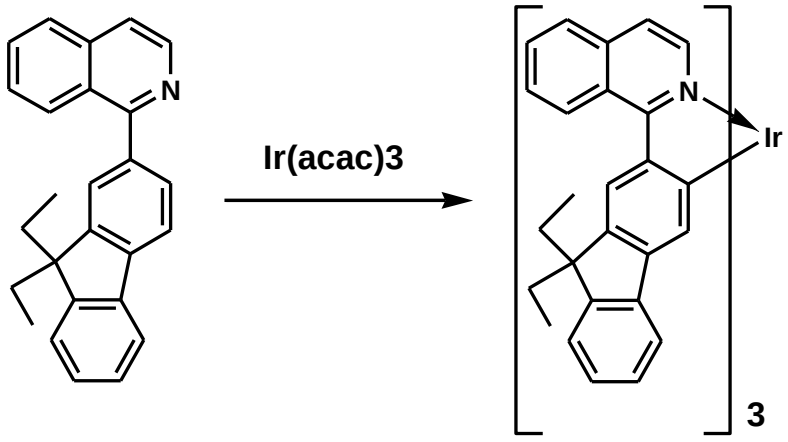

56 **57**

Guoliang *et al*., have demonstrated three NIR-emitting cationic iridium(III) complex.[4] Complex displayed a maximum peak at 698 nm and a shoulder around 760 nm in PL spectra and also acts as phosphorescent dyes for live cell imaging.

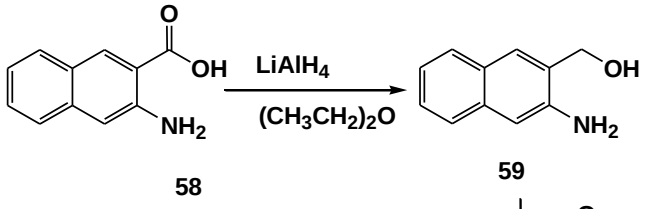

58 **59**

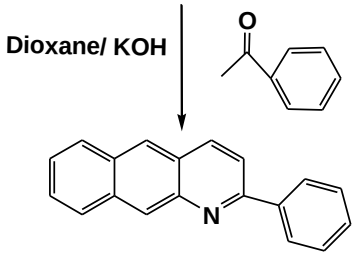

60

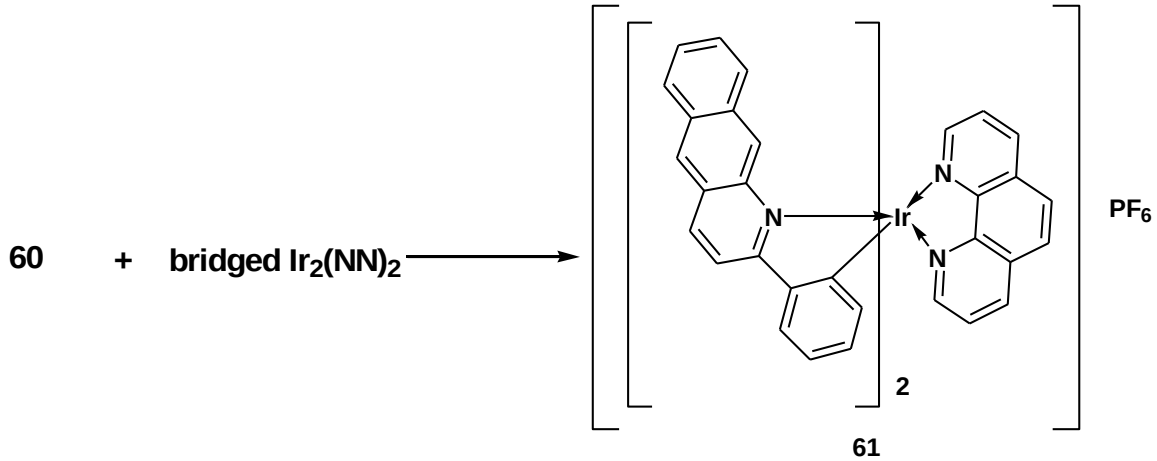

61

Cuisong *et al.,* designed a simple strategy to fabricate optical electrospun fibers doped with an iridium complex[5] sensing surface using electrospinning technique. The luminescence studies revealed that the sensors can quickly detect glucose at the trace level in less than 1second at nanomolar concentration. The study was prolonged to check the reusability, the long-term stability and selectivity of the biosensor.

Soumik Mandal *et al.*,[6] have synthesized and characterized new rhodium and iridium complexes containing 2-phenylpyridine Schiff base ligand, which is capable of cellular imaging. Cyclic voltammetric studies revealed that the complexes undergo one electron oxidation and behave as anodic material. The structure of the complexes was confirmed by X-ray Crystallography.

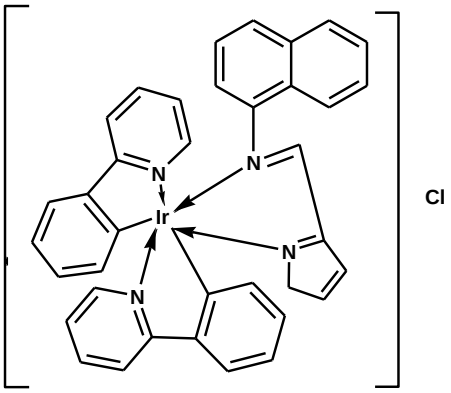

62

Soumik Mandal *et al*.,[7] have reported the fluorescence studies of cyclometalated iridium(III) complexes having bipyridine as ancillary ligand and found that the fluorescence of the complexes depend on the pH. A detailed research was conducted on Ir(III) complexes functionalized nanoparticles with the N,N-diethylamino group in the ancillary ligand to cause photoinduced necrosis.

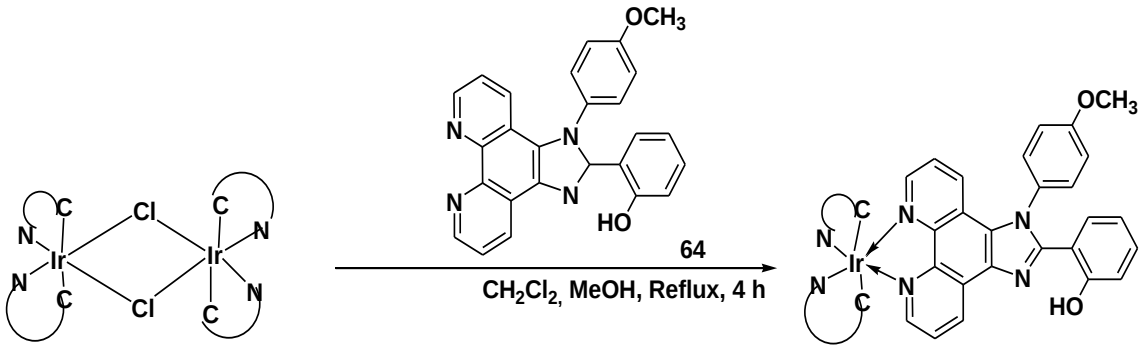

63 **65**

The cyclometalated rhodium and iridium complexes[8] of naphthaldimine-based poly(propyleneimine) dendrimer scaffolds were synthesised by Lara C Sudding. The structures of complexes have been determined by single-crystal X-ray diffraction analysis and *in vitro* anticancer activities of complexes were evaluated against the A2780 and A2780 cisR human ovarian carcinoma cell lines and exhibited significant activity.

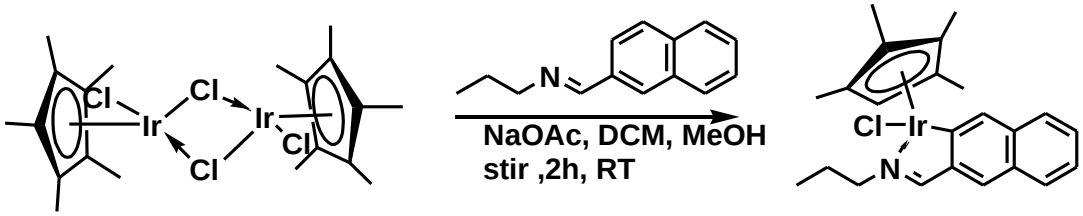

66 **67**

Bezzubov *et al.*, have synthesized and characterized a series of mixed ligand cyclometalated iridium(III) complexes[9] with 2-aryl-1-phenylbenzimidazoles. The UV absorption spectra of the complexes exhibited charge transfer bands in the low energy region and shifted to higher wavelength due to the presence of electron donating power of the ligand. The complexes showed visible luminescence. The complexes showed reversible and quasireversible redox transitions in solutions.

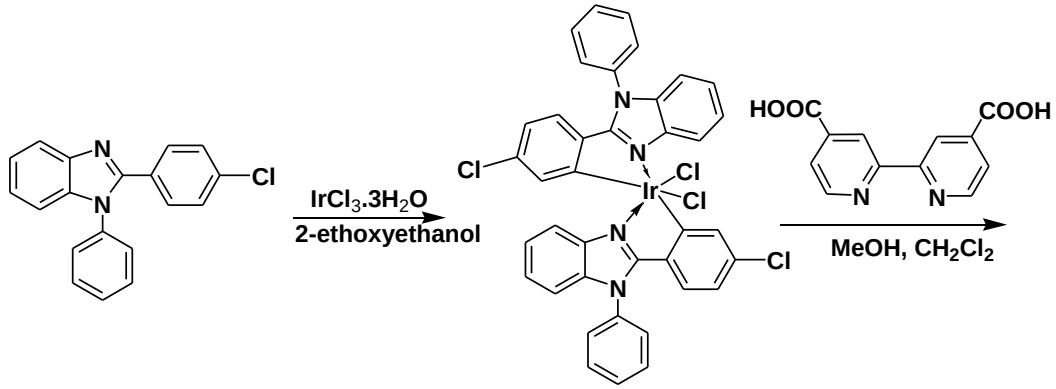

68 **69**

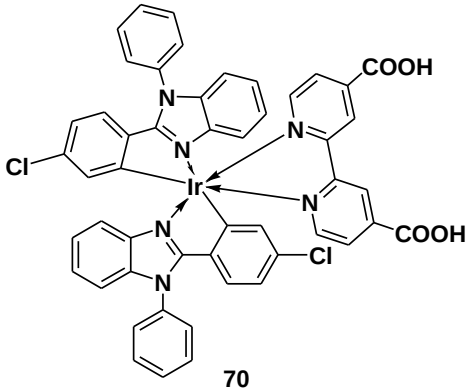

70

Soumik Mandal *et al.,* have reported the synthesis and characterization of two Ir (III) complexes[10] bound with mannose and galactose. The emission studies revealed that the mannose bounded with Ir(III) complexes exhibited good interaction with lectin concanavalin A, whereas galactose bound Ir(III) complexes not show any interaction with lectin.

Cyclometalated rhodium(III) and iridium(III) complexes with imidazolyl modified phenanthroline ligands were synthesized and characterized by Sourav Kanti *et al.*[11] The photophysical studies revealed that the complexes as well as ligands were affected by the solvent polarity and vicinity of the environment.

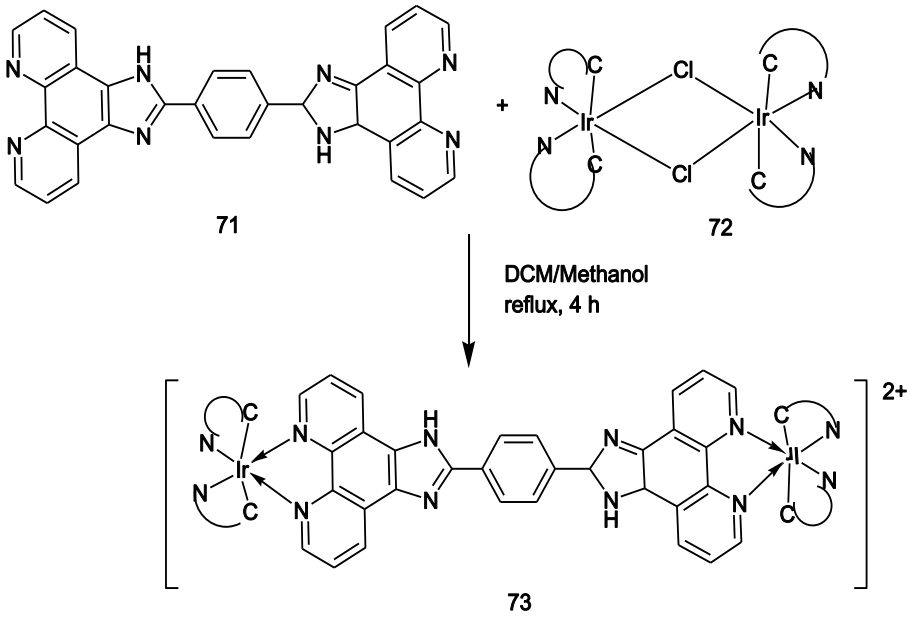

Nakagawa *et al.,* have reported new pH-responsive irdium (III) complexes[12] having aminopyridine ligand. The colour of the complexes were susceptible to pH change. PL spectra of the complexes showed that there is red shift in the emission wavelength, which depends on the substituents. The photo irradiation of complexes at 465 nm caused extensive photo induced necrosis-like cell death of HeLa-S3 cells.

Jayabharathi *et al* .,[13] studied the electroluminescent properties of heteroleptic bis-cyclometalated iridium(III) complexes containing phenanthrimidazole ligands. The iridium complexes exhibit strong phosphorescence emission maxima range from 558 to 574 nm. The quantum efficiency of the complex ranged from 6.5 to 15.6%.

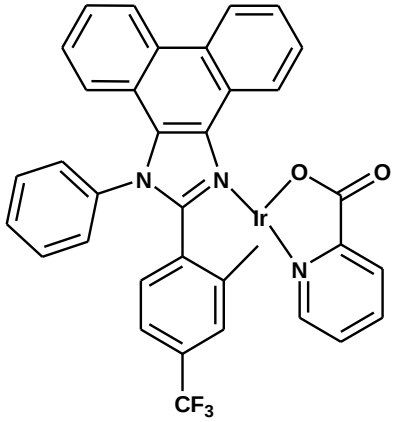

74

Narasinga *et al.*,[14] have synthesised and characterized the mononuclear and dinuclear half-sandwich organometallic rhodium and iridium complexes with picoline ligands. The *in vitro* antitumor evaluation of the complexes by fluorescence based apoptosis study revealed their higher antitumor activity against Dalton's ascites lymphoma cells. The antibacterial evaluation of complexes revealed their significant activity. The docking studies revealed their strong interaction with few key enzymes associated with cancer *viz* ribonucleotide reductase, thymidylate synthase, thymidylate phosphorylase and topoisomerase II. The complexes exhibited a HOMO– LUMO energy gap from 2.95 eV to 3.59 eV, in TDDFT calculations.

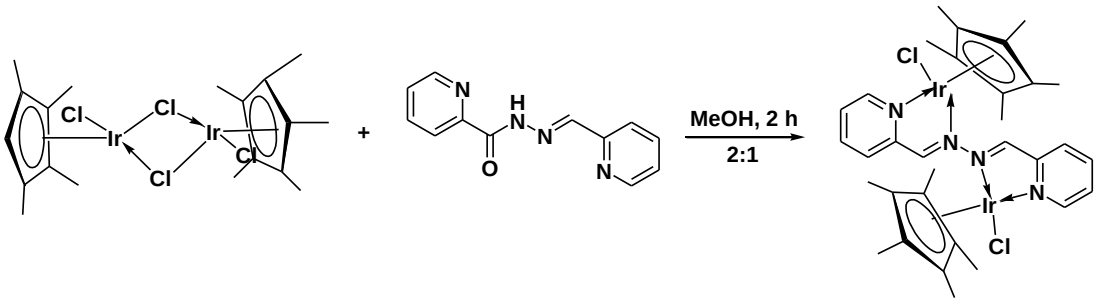

75 **76** **77**

Soumalaya Singh *et al*., have synthesized and characterised two (aryl) ethenyl functionalized 2,2′-bipyridine and their iridium(III) complexes.[15] The photoinduced cis trans isomerization of complexes were evidently proved by quantum chemical calculations.

Lihua *et al*.,[16] have identified that iridium(III) and rhodium(III) complexes selectively inhibit the growth of *S. aureus.* Complexes inhibit the growth of *S. aureus* with MIC and MBC values of 3.60 and 7.19 μM. The complex **78** also showed cytotoxicity against a number of cancer cells.

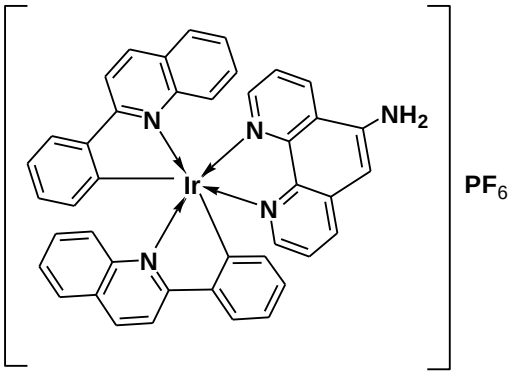

78

Sujay *et al.*,[17] have synthesized and characterized cyclometalated Rh(III) and Ir(III) complexes and the structures of complexes have been authenticated by single-crystal X-ray analyses. The complexes effectively bind with DNA through electrostatic interactions and the molecular docking studies revealed that these complexes bind with the minor groove of DNA. The cytotoxicity studies for the complexes towards the A549 cell exhibited the lowest IC50 value (lower than that of cisplatin), the highest ROS generation at low concentration ($c = 10^{-6}$ μM).

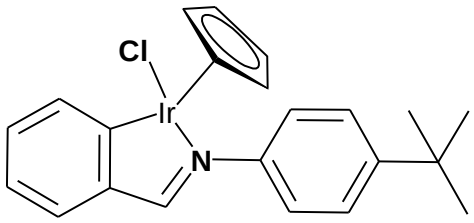

79

Bejoy Mohandas *et al.*, have synthesized, characterized and analysed the photophysical properties of a series of bis(2′,6′-difluoro-2,3′-bipyridinato-N,$C_{4'}$) iridium(picolinate) complexes[18] with different electron-withdrawing (–CHO, $–CF_3$, and –CN) and electron-donating (–OMe and $–NMe_2$) substituents in the bipyridine ring. The emission studies proved that the substituted iridium (III) complexes display excellent emissions in the blue and green regions with high quantum efficiencies. The fabrication of complex **82** fruitfully displayed bright blue emission with luminescence of 33180 cd m^{-2}.

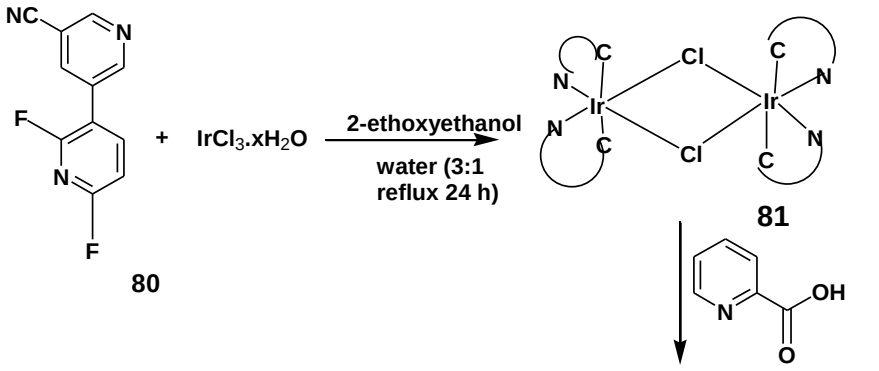

80 81

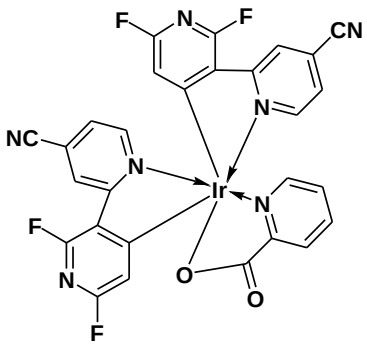

82

Bejoy Mohandas has designed and developed the novel phosphorescent iridium(III) complexes, especially heteroleptic complexes[19] derived from 2,3′ -bipyridine class of cyclometalating and ancillary ligands for various opto- electronic applications. The intriguing photophysical properties of iridium(III) compounds are strongly influenced by the spin-orbit coupling exerted by the iridium(III) core with shortest lifetime.

Parnagupta *et al.*, have reported the optimized structure, electrochemical, quantum chemical and the spectral behavior of homo and hetero dinuclear cyclometalated iridium and rhodium complexes[20] in solution.

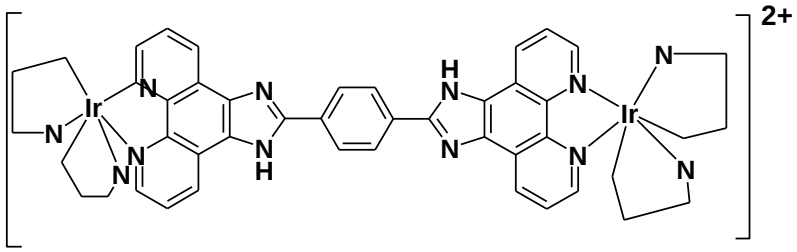

83

The reaction of N-heterocyclic carbenes and aryl-CH bond activation of dinuclear iridium complexes[21] were reported by Miguel *et al.*, The coordination fashion of the

ligands produced from the C−H bond activation processes makes the metal fragment with the ligand more stable NHC chelating system.

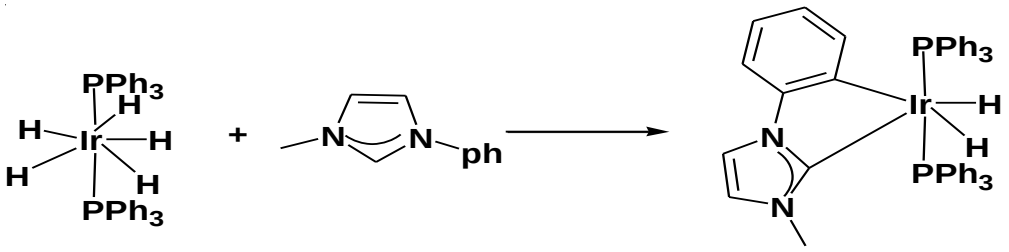

84 **85** **86**

The detailed study of the synthesis, characterization, DNA and protein binding and anticancer activity of organometallic half sandwich Ru(II), Rh(III) and Ir(III) complexes[22] containing 2-(1H-benzo-[*d*]imidazol-2-yl)aniline ligand was done by Amit kumar *et al*., The compounds were found to possess strong interaction with DNA by minor groove mode and act as potent anticancer agent towards SiHa cells.

Melissa V. Werrett *et al.*, have synthesised and characterized Ir(III) tetrazolate complexes[23] and studied their luminescent performance. The luminescence modulation of these Ir(III) complexes shifted the emission color and varied the intensity of the radiative processes.

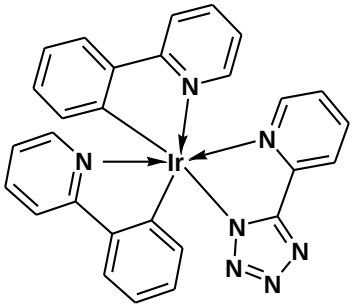

87

Qingcheng Zhao *et al.*, have synthesized graphene oxide doped iridium(III) complex[24] and studied its luminescent property. The complex acts as a excellent biosensor to detect DNA.

Miguel A. Esteruelas *et al.*, carried out a study on the synthesis of a novel family of phosphorescent heteroleptic iridium(III) emitters[25] and their photophysical properties.

These six-coordinate complexes were yellow-orange emissive upon photoexcitation, with short lifetimes and quantum yields in the range 0.04−0.75.

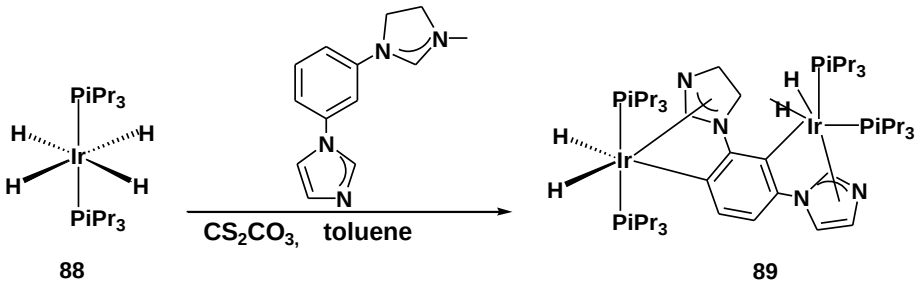

88 89

Shrabanti Das *et al*., have studied the interaction of a cyclometalated dinuclear Ir(III) complex[26] with large and small lipid vesicles in aqueous medium. The emission of the complex is due to triplet metal-to-ligand charge transfer transitions. The weak emission of the complex in aqueous medium increases on interaction with anionic lipid vesicles.

Yuyang Zhou *et al.*, have designed and synthesised a series of iridium complexes[27] containing the ancillary ligand 4-(4′-methyl-[2,2′-bipyridin]- 4-yl)butanoic acid. The coreactant-assisted potential scan experiments found that the iridium complexes could exhibit excellent ECL performance and the ECL efficiency was up to 18 times higher than that of the corresponding ruthenium complex.

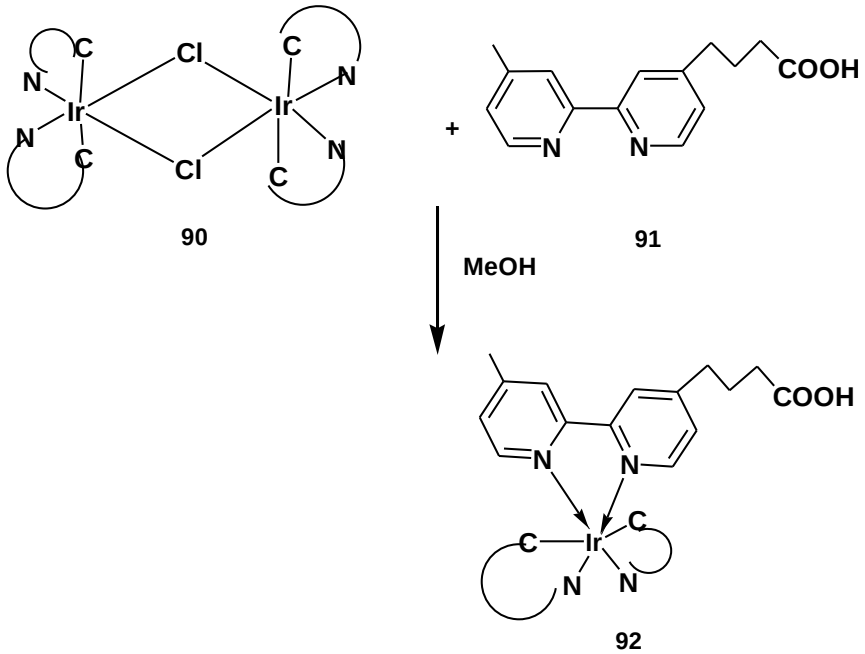

90 91 92

Miao Ouyang *et al* .,[28] have designed and prepared a series of cyclometalated Ir(III) complexes and studied their ability to act as photodynamic therapeutic agents. The complexes showed low cytotoxicity in the dark, while exhibiting prominently high photoinduced cytotoxic activity. Besides, these complexes can penetrate into cancer cells quickly and target mitochondria preferentially. They showed high selectivity between tumor cells and normal cells and satisfying PDT effect towards a cisplatin-resistant cell line (A549R). The complex **94** exhibited the highest quantum yield and highest lipophilicity towards HeLa cells.

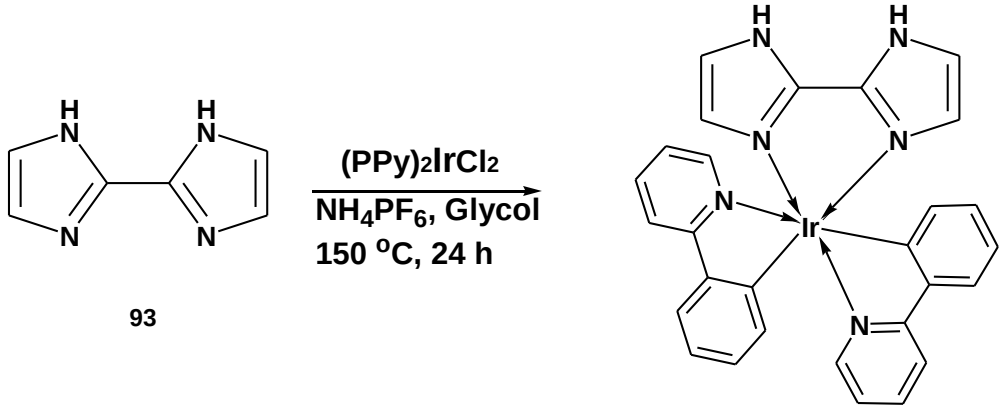

93 **94**

Chunxiang *et al.*, have designed and employed a luminescence reagent bearing cyclometalated iridium complex[29] for cancer cell detection.

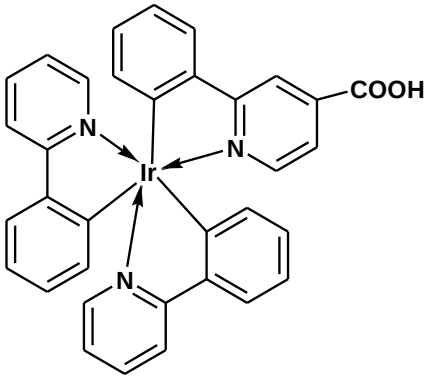

95

A series of cyclometalated iridium complexes[30] having rhodamine moiety was synthesised and characterized by Modi Wang *et al.*, and were used as chemsensors under optimized condition for the reactive and sensitive detection of Cu^{2+} ions.

Xiudan *et al.*, have designed and synthesized iridium complexes[31] and found to be more sensitive in the detection of cyanide ions in the copper salts.

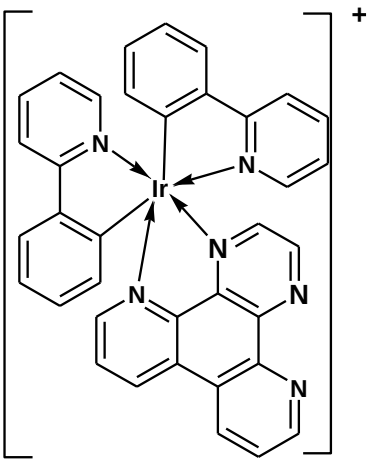

96

Erik Ekengard *et al*., have synthesized and characterized pentamethyl cp-Rh and Ir complexes[32] having chloroquine system. The compounds were screened for their antimalarial activity and found to have moderate activity compared to the standard. The salicyladimine Schiff base containing electron withdrawing substituents exhibited better activity than their counterparts.

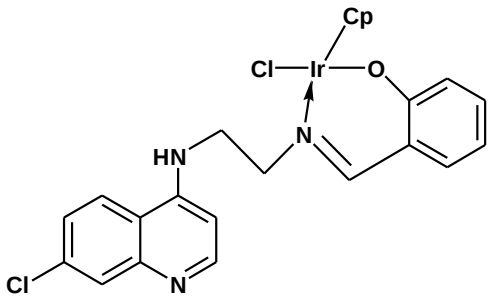

97

Jia Ling Lia *et al*., have synthesized and characterized iridium complexes[33] having pyridine and imidazolylidene chelating system, which act as a tridentate ligand. The structure of the complex was determined by X-ray crystallography. The complexes exhibit good quantum efficiency and electroluminescent capacity. Thus the complexes act as excellent OLED devices.

A series of iridium complexes[34] containing napthyridine derivatives have been synthesized and characterized by Sanjay Adhikari *et al*. The compounds were screened for anticancer activities and found to possess better activity.

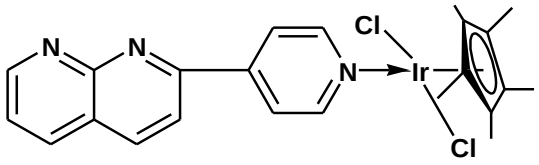

98

2.2. Results and Discussion

Iridium (III) complexes have been emerging as an alternative to platinum based drugs[35] due to their solubility, liability towards the exchange of ligands and good cytotoxicity against cancer cell line.

Apart from the pharmaceutical importance, Ir(III) complexes have been employed as sensors and OLED devices[36,37] due to their fascinating photophysical properties, quantum yields, stokes shifts and as long lived excited species.

The widespread importance of pharmaceuticals and industrial applications of Ir(III) complexes has intended us to synthesise novel iridium (III) complexes with hydrazino and thiosemicarbazinoquinoline Schiff bases **11(a-d)** and **13(a-d)** respectively.

2.2.1. Synthesis of Ir(III) complex (14a)

Accordingly, equal moles of ligand 4-methyl-2-(salicylidenehydrazino) quinoline**(11a)** and $IrCl_3.3H_2O$ were dissolved in ethanol and refluxed for six hours with periodic monitoring with TLC. As the color of the reaction mixture changes from greenish yellow to yellow color, completion of the reaction was confirmed by TLC. An yellow colour solid separated as the contents were cooled. The product obtained was recrystallized from ethanol/chloroform mixture. Yield : 0.43 g(56%), M.pt- >200 ^oC

With the perceptions obtained from the DFT studies, the expected mode of coordination sites available in the ligand **11a** are $^{32}N^{17}N^{30}O$, $^{32}N^{15}N^{30}C$ and $^{17}N^{12}C^{30}O$ sites.

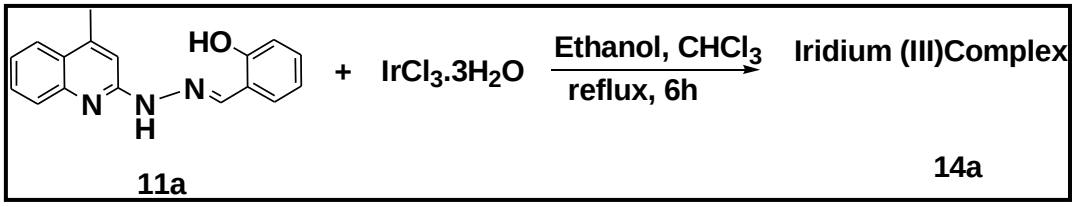

The Conductance value of iridium complex **14a** was measured by using DMSO in 10^{-5} concentration. Using this value, the molar conductance was calculated and found to be 25 ohm^{-1} cm^2 mol^{-1}. The low value indicates the non – electrolytic nature of the complex.

IR (cm^{-1}) (υ_{max}) fig (60): Compound **14a** displayed bands at 3386, 3010, 1541, 1092 are assigned to –OH, -NH, -C=N and –C-O respectively.

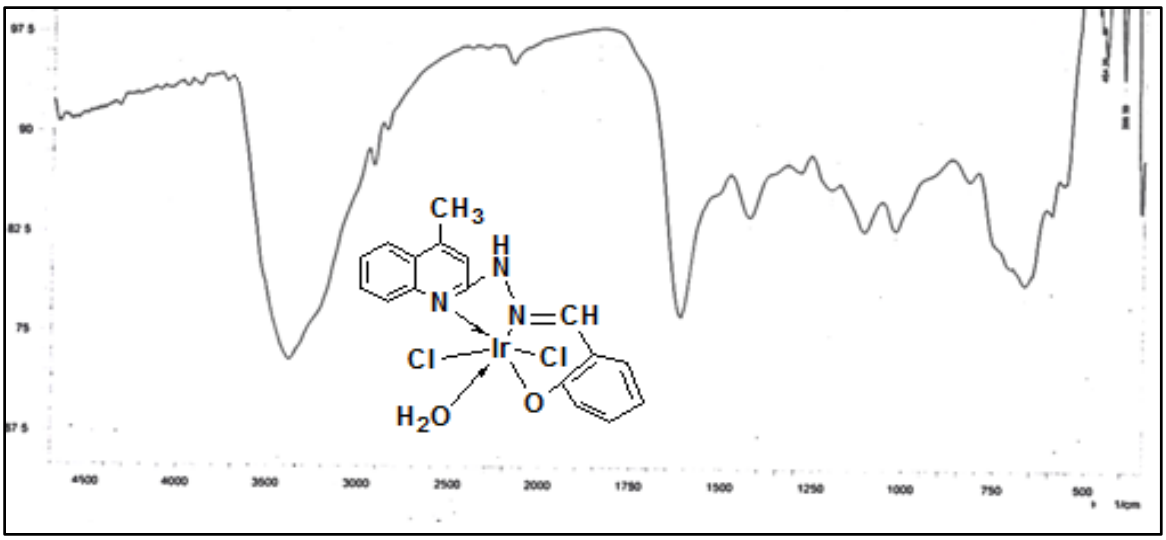

Fig 60 - IR spectrum of Iridium (III) complex 14a

On comparing the IR spectrum of ligand **11a**, a shift from 1610 cm^{-1} to 1541 cm^{-1}, 1263 cm^{-1} to 1092 cm^{-1} and also a broad absorption at 3386 cm^{-1} noticed in the IR spectrum of compound **14a** indicates the coordination of the metal through oxygen of C-O, N of –C=N of the quinoline ring and –NH of hydrazine azomethine.

^{1}H-NMR ($CDCl_3$) (ppm) fig (61): Compound **14a** δ 11.4 (s, NH), δ 5.6 (s, OH), δ7.5 – 7.0 (m, nine aromatic and one azomethine protons), δ 2.4 (s,–CH_3). The signal for methyl protons appeared around δ 1.2ppm. The disappearance of phenolic –OH peak at 9.0 ppm of the ligand **11a** and appearance of signals at 5.6 ppm indicates the presence of coordinated water molecules. The signal appeared in the range of 11.4 was assigned to NH-. The peak at δ δ7.5-7.0 ppm corresponds to aromatic and azomethine protons of the metal complex **14a.**

The shift of NH- resonance from δ 10.8 to δ 11.4 ppm, clearly explains the electron density of –NH of ligand **11a** is donated to metal atom thereby it is more deshielded than ligand. From the data it is confirmed that the ligand is coordinated through C-O of phenolic group, -N of quinoline ring and -CH=N to the metal.

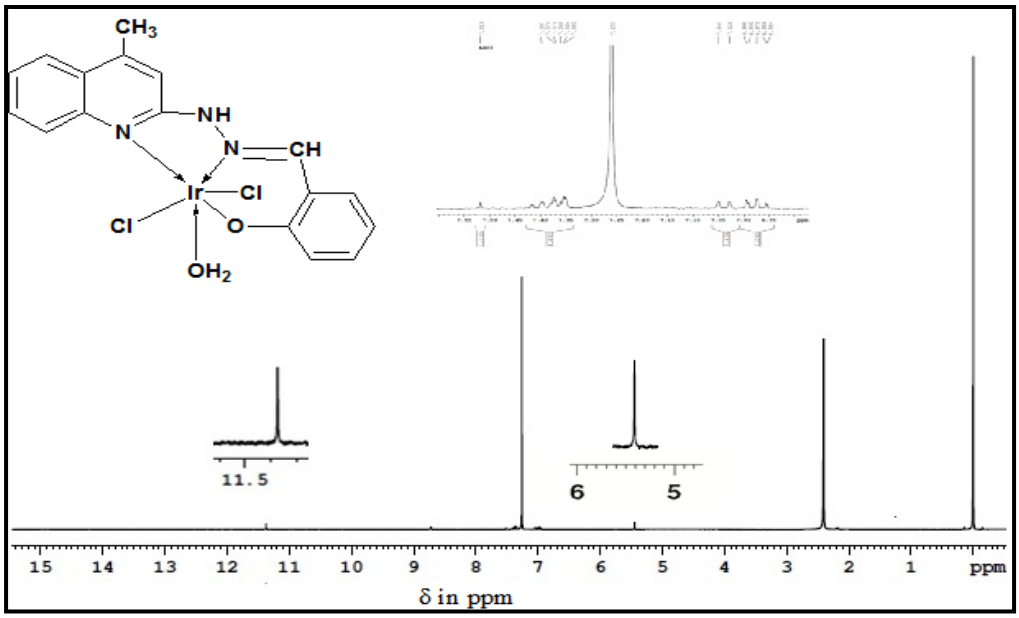

Fig 61 - ^{1}H NMR spectrum of Iridium (III) complex 14a

UV spectrum λ_{max}(nm) (fig 62): Compound **14a** displayed three absorption bands in the region of 270 nm, 441 nm and 570 nm. The UV absorption spectrum exhibited high energy, intense and broad band at 270nm which is fundamentally assigned to spin allowed $^{1}(\pi\text{-}\pi^{*})$ transitions of the ligand.[38] The low energy band at 441 nm is due to MLCT (metal-to-ligand charge transfer) transition and the band at 570 nm is due to greater charge transfer caused by the mixing of metal and ligand orbital contributing to $^{1}A_{1g} \rightarrow {}^{1}T_{2g}$, $^{1}A_{1g} \rightarrow {}^{1}T_{1g}$ and $^{1}A_{1g} \rightarrow {}^{3}T_{1g}$ transitions. This pattern of the spectrum indicates octahedral geometry around the metal ion.

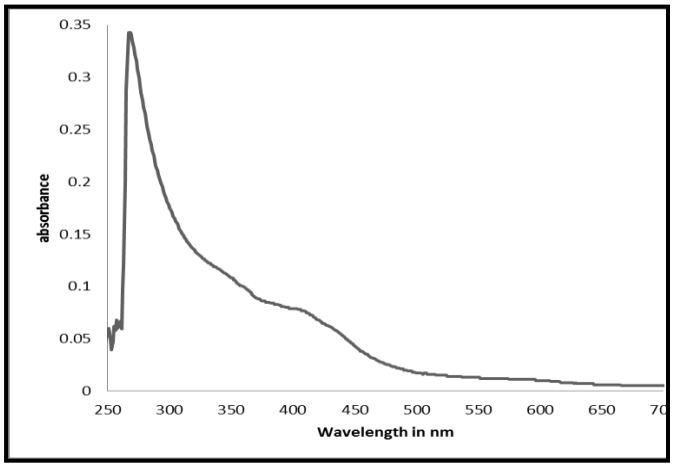

Fig 62 - UV spectrum of Iridium (III) complex 14a

From the UV spectrum, it was concluded that the iridium complex possess distorted octahedral geometry.

The **cyclic voltammogram** of Ir(III) complex **(14a)** in acetonitrile medium shows one distinct coupled peak conforming to $Ir^{III/II}$ and $Ir^{II/III}$ **(fig 63)**. The cathodic peak potential is -0.487V corresponds to the one electron reduction of Ir(III) and the corresponding anodic peak potential is 1.30V. The ΔEp value (831mV) of the complex indicates that these redox couples are quasi-reversibile. The ratio of the cathodic and anodic peak current is nearly unity and indicates one electron transfer in this redox process.[39]

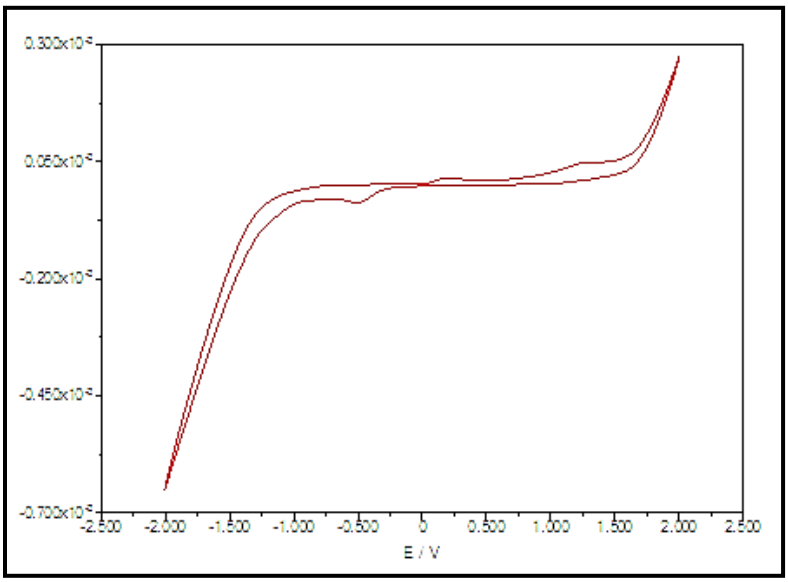

Fig 63 - Cyclic Voltammogram of Iridium (III) complex 14a

The thermogravimetric studies of complex **14a** was carried at the heating rate of 20 ºC min^{-1} under nitrogen atmosphere and weight loss as measured from the ambient temperature upto 730 ºC.

The TGA curve of the metal complex[40] **14a** shows three stage decomposition. Since there is no decomposition around 100 ºC, it is clear that there are no free water molecules and the expected water molecules are present inside the coordination sphere. This was confirmed by the decomposition peak position observed at 308 ºC along with the loss of one water molecules and two chlorine atoms with the % composition of 17 % (M-88).

The second decomposition at the temperature 476 ^{o}C with a 40% loss corresponds to the decomposition of the ligand moiety of the complex **14a**. The remaining residue left founds no further decomposition till 730 ^{o}C, might be corresponds due to the metal oxide. (43%)

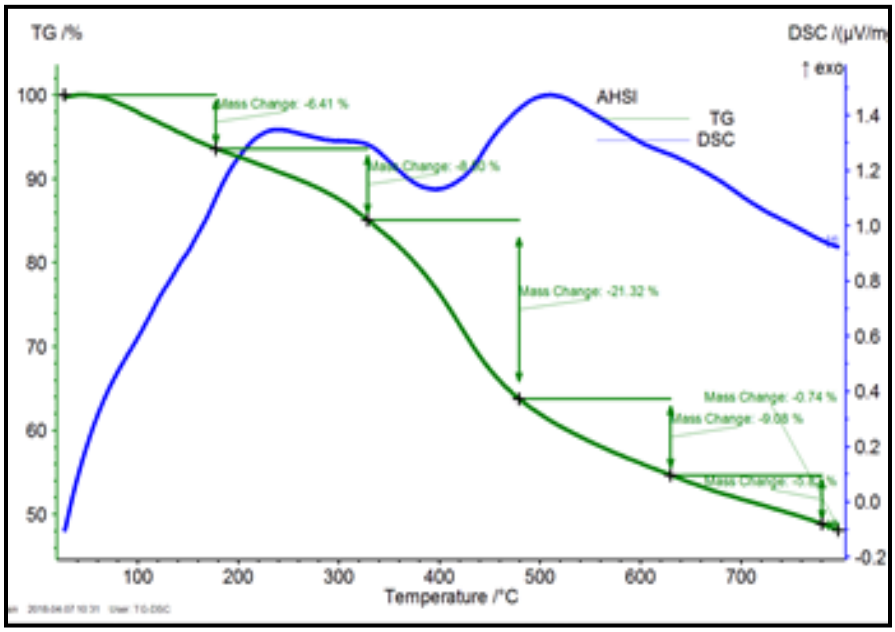

Fig 64 - TGA curve of iridium (III) complex 14a

Simultaneously DSC curve shows that the decomposition of metal complex involves two exotherms and one endotherm.

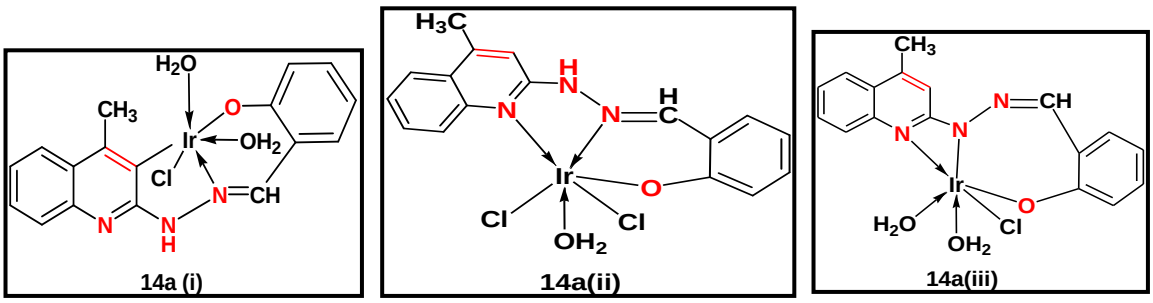

Among the suspected structures **14a(i), 14a(ii)** and **14(iii),** The structure of **14a(ii)** are found to be well in line with the spectral and analytical data.

The crystal lattice parameters of the iridium complex **14a** are calculated using fullprof suite program.[41] The parameter of the complex **14a** were found to be a=7.915, b=18.4558, c=14.2421, α=90.000, β = 95.025, γ=90.00 and these showed that the complex **14a** belongs to the monoclinic crystal **(fig 64a).**

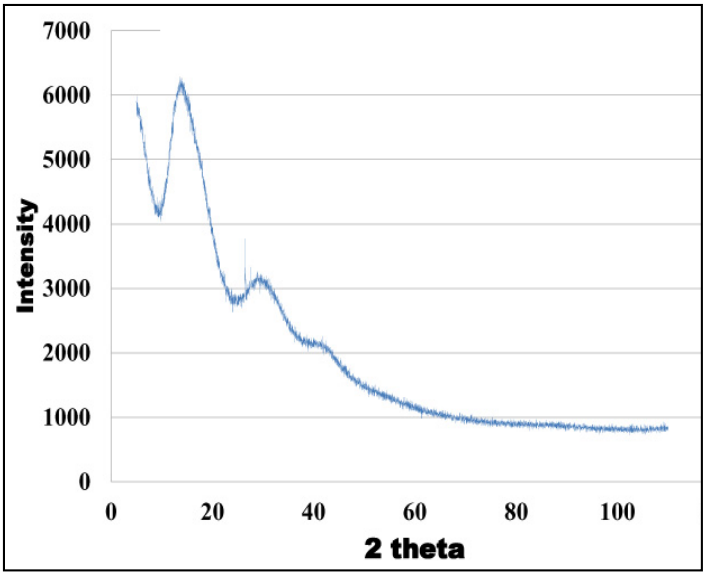

Fig 64a - XRD pattern of iridium complex 14a

Hence the synthesised novel iridium(III)complex expected to have an octahedral geometry and with NNO mode of coordination by the quinoline ligand.

The reaction sequence has been extended to synthesise **14(b-d)** following the same reaction and workup procedure. The spectral and analytical data of these complexes fall well around the ranges explained. The structures of the derivatives are given in **chart III.**

Chart III

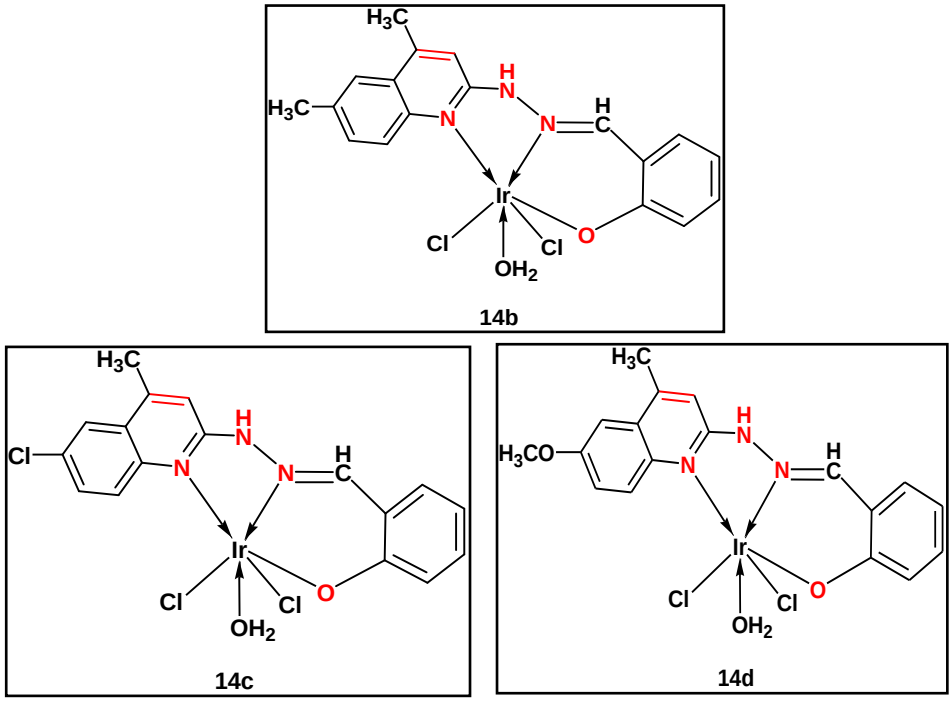

After achieving the iridium (III) hydrazino Schiff base, next we thought of extending the reaction with thiosemicarbazone Schiff base ligand and thereby to study their coordination.

2.2.2. Synthesis of Ir(III) complex (15a)

Equal moles of $IrCl_3.3H_2O$ (0.5 g) and 4-methyl-2-(salicylidene thiosemicarbazino)quinoline (0.5 g) in ethanol medium was refluxed in a water bath for 24 h and the completion of the reaction was checked by TLC. After the completion of the reaction, the reaction mixture was concentrated and the crude obtained was recrystallized from ethanol/chloroform mixture. A yellow coloured amorphous powdered with an yield of 0.43 g (54 %) was obtained. M.pt 200^oC

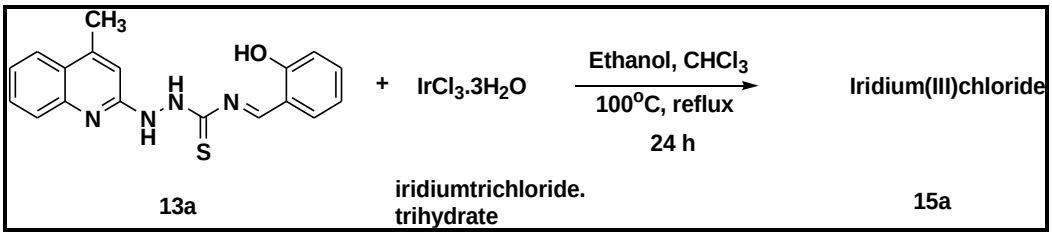

Scheme 7

The molar conductance of the complex 15a (10^{-5} M, DMSO medium) was found to be 63 $ohm^{-1}cm^{2}mol^{-1}$ and it is non-electrolytic in nature.

IR (cm^{-1}) (υ_{max}) fig (65): Compound **15a** showed bands at 3122(υO-H), 3027 (υN-H), 2950 (υN-H), 1591(υC=N), 1507 (υC=N), 1365 (υC=S), 1190(υC-O).

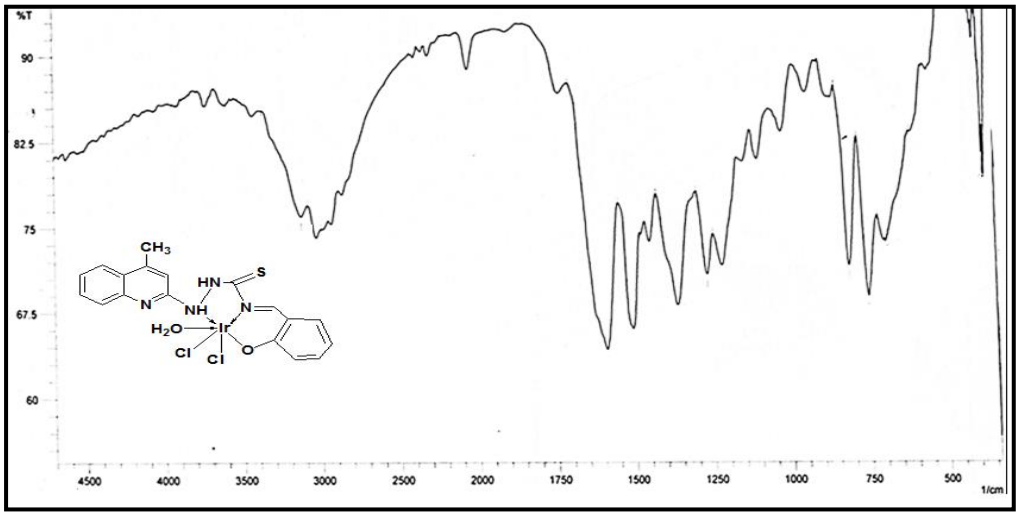

Fig 65 - IR spectrum of iridium (III) complex 15a

There is a pronounced shift in wave numbers of υN-H and υC=N compared to that of the ligand **13a** suggested the coordination to the metal might occur through the –NH groups and azomethine group. The peak assigned for –C=S group did not show any noticeable shift which infers the inertness of –C=S group in the complexation.

^{1}H-NMR ($CDCl_3$) (ppm) fig (66): Compound **15a** resonates at δ 7.7 - δ 6.5 ppm assigned to aromatic protons and azomethine proton. The methyl protons of the complex **15a** appeared as singlet at δ 2.4 ppm. The Peak at δ 11.4 ppm and δ 9.8 ppm were attributed to -NH groups. The disappearance of phenolic –OH peak at δ 9.8 ppm and appearance of broad signal at δ 5.9 ppm indicate the presence of coordinated water molecules.

The peak at δ 10.2 ppm corresponds to -NH of the ligand **13a** shifted downfield to δ 11.4 ppm in the complex **15a**, since the electron density around nitrogen atom is donated to the central metal ion. From the spectral data, it is confirmed that the ligand is coordinated through C-O, -NH and -C=NH to the metal.

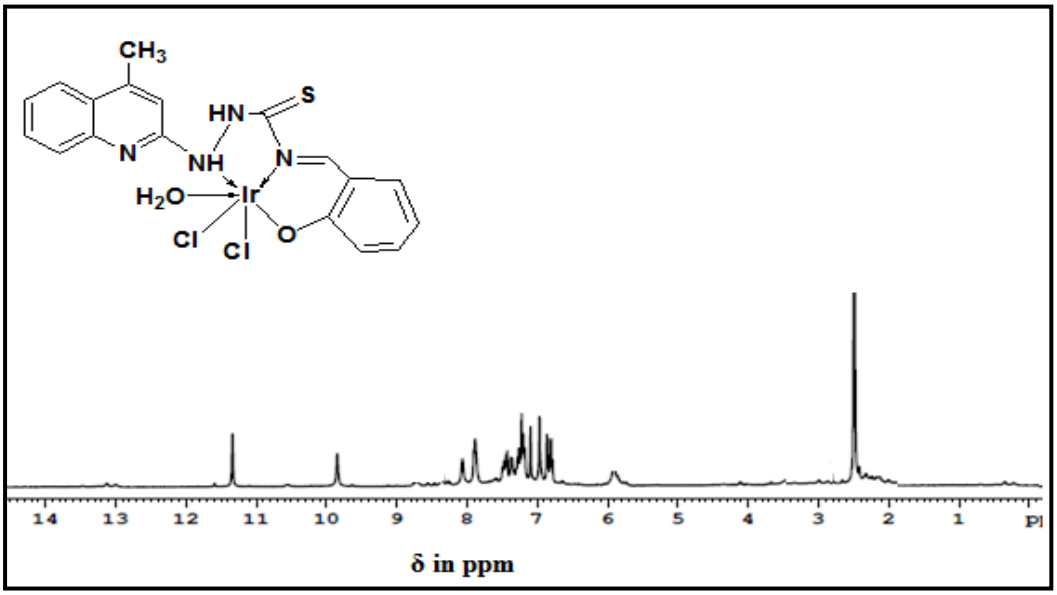

Fig 66 - ^{1}H-NMR spectrum of Iridium (III) complex 15a

The absorption spectrum of the Ir(III) complex **15a** (**fig 67)** presented bands at 277 nm, 417 nm and 586 nm.

The band at 277 nm is ascribed to ^{1}LLCT transitions. In addition, these band at 417 nm is due to the contribution of spin allowed ^{1}MLCT and ^{1}LC transitions. The low

intense band resonance above 450nm is due to spin forbidden singlet to triplet, metal to ligand charge transfer and the strong spin orbit coupling effects of iridium atom of the complex.

From the UV spectral analysis, it was found that the iridium (III) complex has octahedral geometry.

The cyclic voltammogram of Ir(III) complex **15a** in acetonitrile medium shows cathodic reduction potential peak at -0.197 V and anodic oxidation peak potential at 0.795 V, thereby ΔEp value (598 mV) of the complex concludes that Ir (III) complex **15a** is a quasi-reversible system.

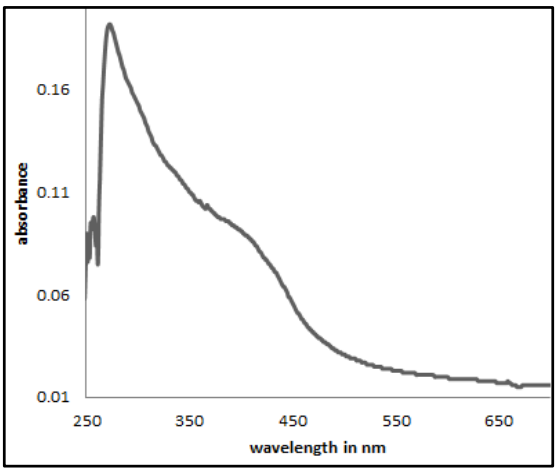

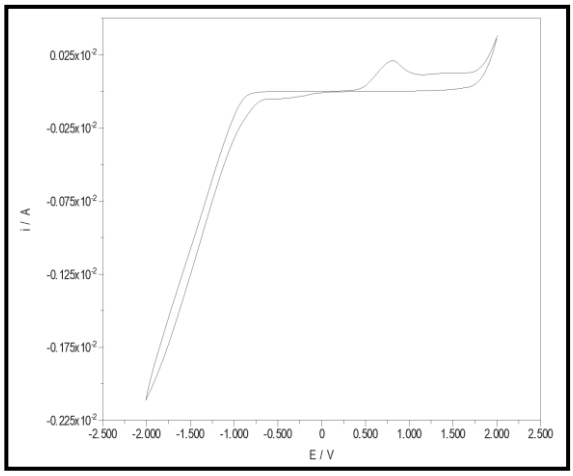

Fig 67 UV spectrum(15a) **Fig 68 CV curve of iridium (III) complex 15a**

The TGA curve of metal complex **15a** showed three stage decomposition **(Fig 69).** The first decomposition obtained in the temperature range 200 ºC (3 %) indicates the loss of one coordinated water molecule. The second stage decomposition was obtained in the temperature range of 305 ºC. The percentage weight loss is in the range of 12 % because of loss of two chlorine atoms with the gradual decrease in the temperature, at 700 ºC the ligand decomposition occurs leaving the metal residue as iridium oxide (44%).

As there is no decomposition around 100ºC, lattice water molecules are absent in the complex.

Two endothermic and one exothermic process are observed in DSC curve.

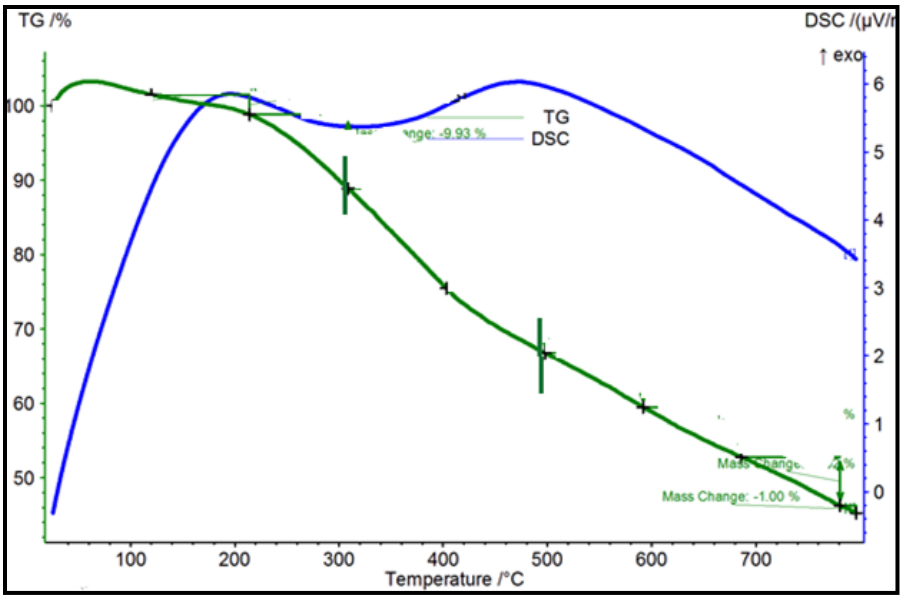

Fig 69 - TG and DS curve of Iridium (III) complex 15a

The crystal lattice parameters of the iridium complex **15a** were calculated and found to be a=7.9010, b=18.4655, c=14.3158, α= 90.000, β= 84.959, γ =90.00 and it falls in the monoclinic crystal system **(fig 70)**.

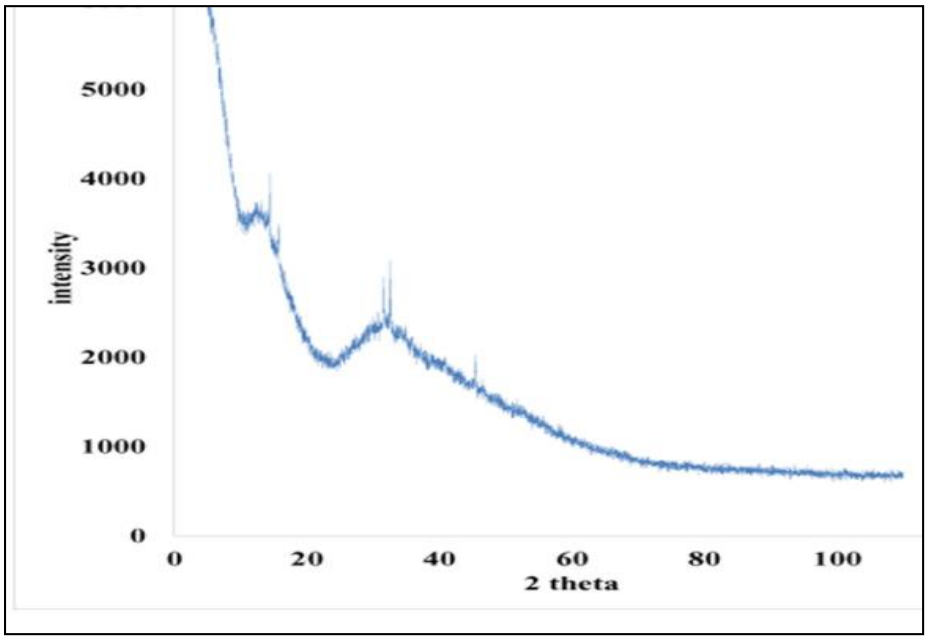

Fig 70 - XRD curve of iridium complex 15a

From the analytical and spectral data, the structure of complex **15a** is

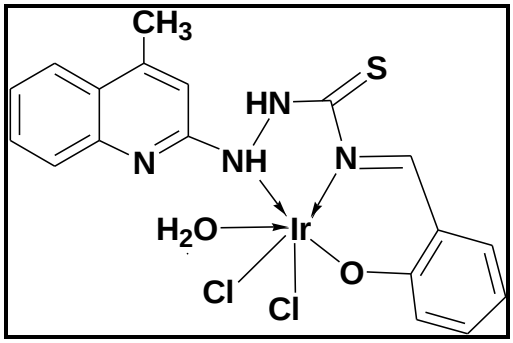

The reaction is extended to its derivatives **15(b-d)** and the spectral data were similar to that of **15a,** therefore it is concluded that the derivatives possess similar structures **(chart IV).**

Chart IV

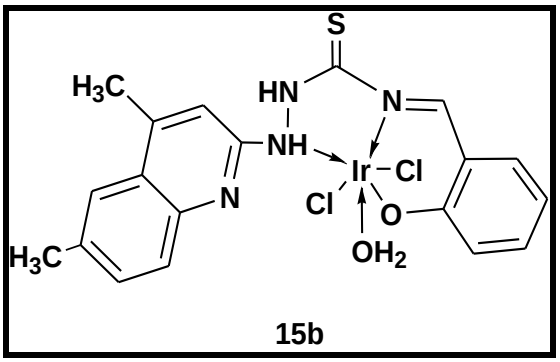

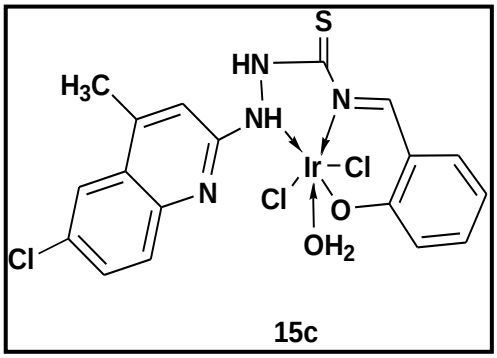

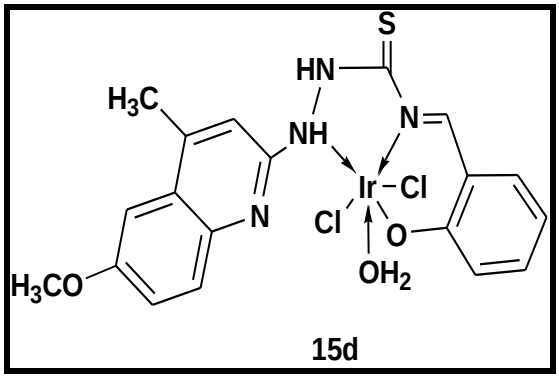

Further the formation of complexes **14a** and **15a** were cross verified with the theoretical evaluation of the structure confirmed by DFT / B3LYP 631G* (d,p) basis set.

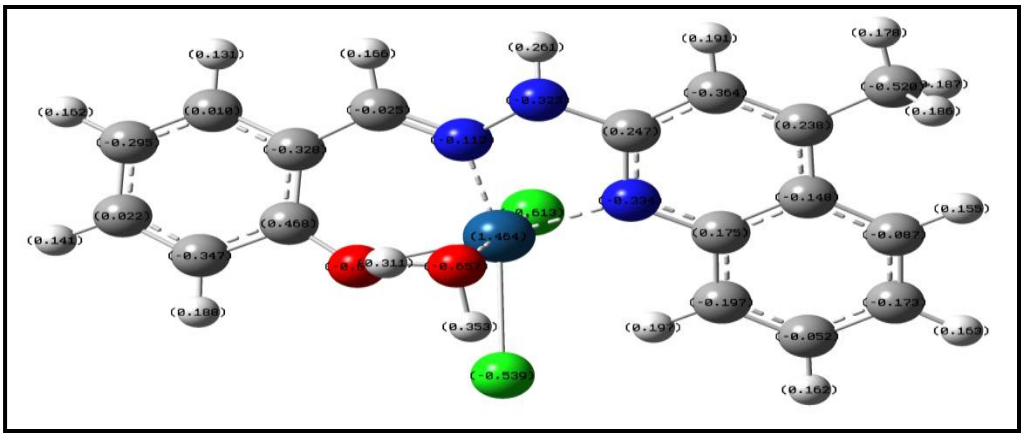

Fig 71a - Optimised geometry of complex 14a

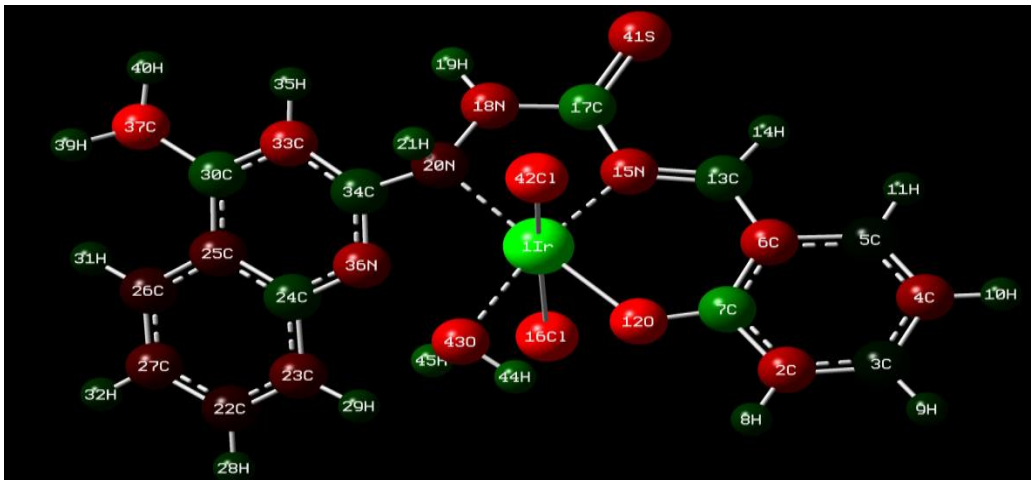

Fig 71b - Optimised geometry of complex 15a

The Mulliken charge of the atom obtained from optimized geometry (**71a** and **71b**) for the complexes **14a** and **15a** are compared with the corresponding ligands. **11a** and **13a** (**Table 11**)

The charges on the atoms which are supposed to be the coordination sites have decreased accordingly at the expected sites of the coordination. (**Table 11**).

DFT studies also support the proposed structures of complexes **14a** & **15a.**

MEP **(fig 72a and 72b)** showed their shift in the electron density between the ligand and the complex. The Energy gap between HOMO and LUMO of the complex was comparatively higher than that of the ligand.

Table 11: Comparison of Mulliken charges of metal complexes 14a & 15a and ligands 11a and 13a

Atom 11a	Mulliken charge	Atom 14a	Mulliken charge	Atom 13a	Mulliken charge	Atom 15a	Mulliken Charge
15N	-0.487	15N	-0.323	20N	-0.490	20N	-0.151
30O	-0.559	30O	-0.657	25N	-0.545	15N	-0.409
32N	-0.655	14N	-0.334	38O	-0.556	12O	-0.576

Table 12: Energy parameters of complexes 14a & **15a**

In eV	14a	14b	14c	14d	15a	15b	15c	15d
HOMO	-7.01	-6.80	-6.91	-7.03	-6.99	-6.91	-7.06	-6.97
LUMO	-2.49	-2.45	-2.56	-2.45	-2.52	-2.51	-2.60	-2.50
ΔE	4.52	4.35	4.35	4.58	4.47	4.40	4.46	4.47

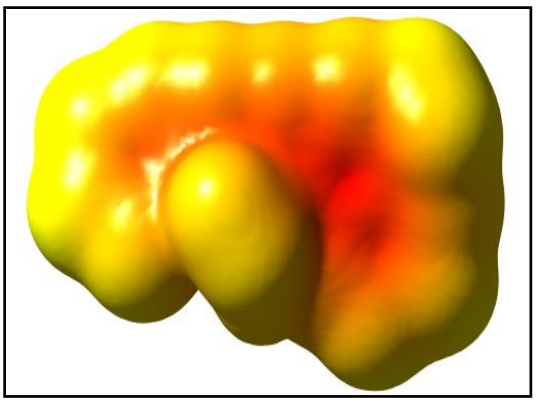

Fig 72 a- MEP diagram of complex 14a

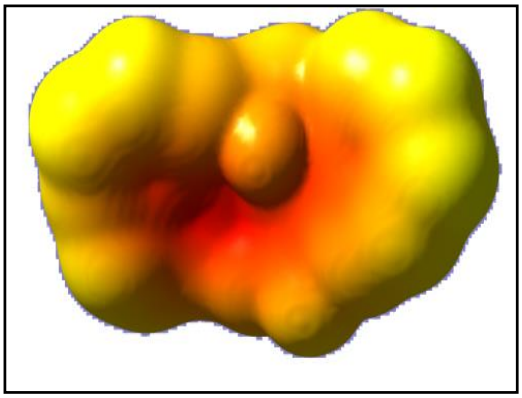

Fig 72b - complex 15a

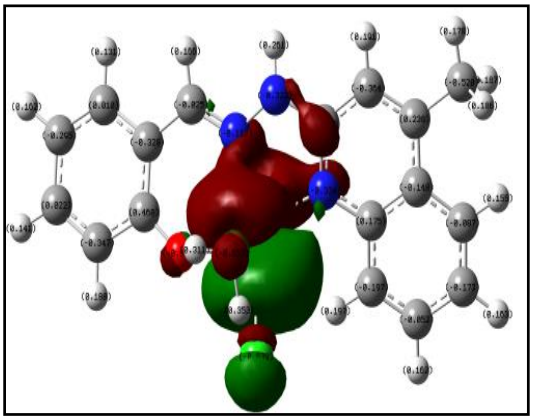

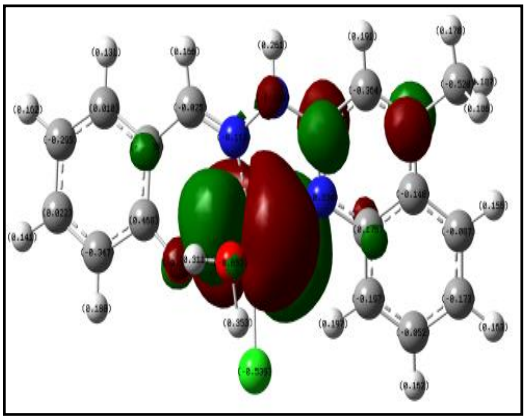

Fig 73 – HOMO and LUMO structures of complex 14a

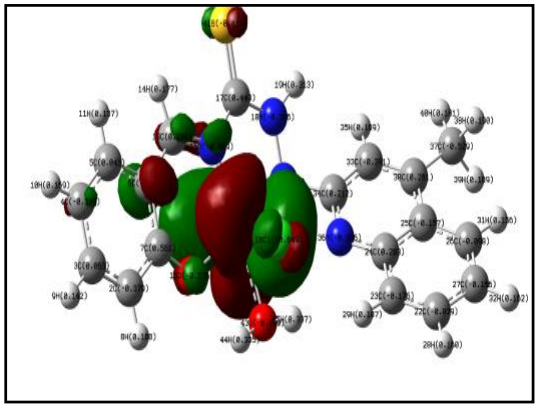

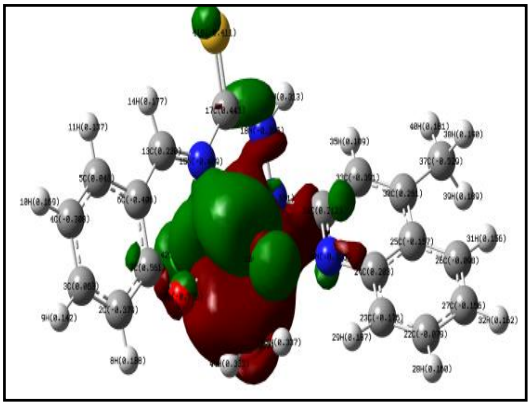

Fig 74 - HOMO and LUMO structures of complex 15a

2.3. Experimental

General Procedure for the preparation of iridium(III)complexes

A hot ethanolic solution of 4-methyl-2-(salicylidenehydrazino) substituted quinoline / 4-methyl-2-(salicylidene thiosemicarbazino) substituted quinoline ligands was added slowly to ethanolic solution of $IrCl_3.3H_2O$ (0.5 g, 1.42 mmol) with continuous shaking. The color changed from yellowish green to intense color during addition. Then it was heated under reflux for about 6-24 h. The solid product was precipitated out. It was filtered and washed with petroleum ether and recrystallized with chloroform/ethanol mixture.

2.3.1. Preparation of Ir(III) complex 14b

Iridium trichloride trihydrate	: 0.5 g (1.42 mmol)
4,6-dimethyl-2-(salicylidenehydrazino) quinoline	**:** 0.42 g (1.42 mmol)
Ethanol	**:** 60 mL
Color	**:** Reddish brown
Yield	**:** 0.45 g (57%)

M.pt >300 ^oC, Anal. calcd for $C_{18}H_{18}N_3O_2Cl_2Ir$: C, 40.44; H, 3.37 ; N, 7.86 %, Found: C, 40.8 ; H, 4.2 ; N, 7.2 %.

IR (cm^{-1}) (υ_{max}) (fig 75) compound **14b:** 3386 (υ_{O-H}), 3100 (υ_{N-H}), 1613 ($\upsilon_{C=N}$ of quinoline ring), 1427 ($\upsilon C=N$), 1110 (υ_{C-O}),

^{1}H NMR (DMSO) (ppm) (fig 76) compound **14b:** δ 8.9 (s, NH), δ 5.4 (s, OH), δ 7.3 – δ 6.8 (m, 9H aromatic and 1H azomethine protons), δ 2.5 (s,–CH_3).and δ 3.4 (s,–CH_3).

2.3.2. Preparation of Ir(III) complex 14c

Iridium trichloride trihydrate	: 0.5 g (1.42 mmol)
4-methyl-6-chloro-2-(salicylidenehydrazino) quinoline	**:**0.45 g (1.42 mmol)
Ethanol	**:** 60 mL
Color	**:** Yellow
Yield	**:** 0.41 g (50%)

M.pt >300 ºC**.** Anal. calcd for $C_{17}H_{15}N_3O_2Cl_3Ir$: C, 36.82 ; H, 2.70 ; N, 7.58 %, Found: C, 36.5 ; H, 2.16 ; N, 7.05 %.

IR (cm^{-1}) (υ_{max}) (fig 77) compound **14c:** 3388 (υ_{O-H}), 3220 (υ_{N-H}) 1536 ($\upsilon_{C=N}$), 1095 (υ_{C-O}).

2.3.3. Preparation of Ir(III) Complex 14d:

Iridium trichloride trihydrate	**:** 0.5 g (1.42mmol)
4-methyl-6-methoxy-2-(salicylidenehydrazino) quinoline	**:** 0.44 g (1.42mmol)
Ethanol	**:** 60 mL
Color	**:** Greenish brown
Yield	**:** 0.39 g (48%)

M.pt >300 ºC, Anal. calcd for $C_{18}H_{18}N_3O_3Cl_2Ir$: C, 39.27 ; H, 3.27 ; N, 7.63 %, Found: C, 40.9 ; H, 4.0 ; N, 7.5 %.

IR (cm^{-1}) (υ_{max}) (fig 78) compound **14d:** 3129 (υ_{O-H}), 3029 (υ_{N-H}). 1602 ($\upsilon_{C=N}$), 1527 ($\upsilon_{C=N}$), 1110 (υ_{C-O}).

2.3.4. Preparation of Ir(III) complex 15b:

Iridium trichloride trihydrate	**:** 0.5g (1.42 mmol)
4,6-dimethyl -2-(salicylidenethiosemicarbazino)quinoline	**:** 0.52g (1.42 mmol)
Ethanol	**:** 60 mL
Color	**:** Greenish yellow
Yield	**:** 0.46g (51%)

M.pt > 300 ºC. Anal. calcd for $C_{19}H_{19}N_4O_2SCl_2Ir$: C, 38.4 ; H, 3.2 ; N, 9.4; S, 5.3 %, Found: C, 38.8 ; H, 3.6 ; N, 8.9 ; S, 5.1 %.

IR (cm^{-1}) (υ_{max}) (fig 79) compound **15b:** 3300(υ_{O-H}), 3100 (υ_{N-H}), 2999 (υ_{N-H}), 1610 ($\upsilon_{C=N}$), 1410($\upsilon_{C=S}$), 1035 (υ_{C-O}).

^{1}H NMR (DMSO) (ppm) (fig 80) compound **15b:** δ 11.4 (s, NH), δ 9.2 (s, NH), δ 8.0 (s, (-N=CH), δ (s, -OH), δ 7.7 - δ 6.5 (m, aromatic protons), δ 3.3 (s, $-CH_3$) and δ 2.4 (s, $-CH_3$) .

2.3.5. Preparation of Ir(III) complex 15c

Iridium trichloride trihydrate	**:** 0.5 g (1.42 mmol)
4-methyl-6-chloro-2-(salicylidenethiosemicarbazino)quinoline	**:** 0.54 g (1.42mmol)
Ethanol	**:** 60 mL
Color	**:** Greenish brown
Yield	**:** 0.41g (44%)

M.pt > 300 ºC. Anal. calcd for $C_{18}H_{16}N_4O_2SCl_3Ir$: C, 35.2 ; H, 2.6 ; N, 9.1 ; S, 5.2 %, Found: C, 35.5 ; H, 2.4; N, 9.5 ; S, 5.14 %.

IR (cm^{-1}) (υ_{max}) (fig 81) compound **15c:** 3381 (υ_{O-H}), 2979 (υ_{N-H}), 2926 (υ_{N-H}), 1605(υ_{C-N}), 1512(υ_{C-N}), 1293 ($\upsilon_{C=S}$), 1166 (υ_{C-O}).

2.3.6. Preparation of Ir(III) complex 15d

Iridium trichloride trihydrate	**:** 0.5 g(1.42 mmol)
4-methyl-6-methyl-2-(salicylidenethiosemicarbazino)quinoline	**:** 0.54 g (1.42 mmol)
Ethanol	**:** 60 mL
Color	**:** Brown
Yield	**:** 0.37 g (40%)

M.pt >300 ºC, Anal. calcd for $C_{19}H_{19}N_4O_3SCl_2Ir$: C, 37.43 ; H, 3.11 ; N, 9.1; S, 5.2 %, Found: C, 38.8 ; H, 3.6 ; N, 9.8;S, 5.9 %.

IR (cm^{-1}) (υ_{max}) (fig 82) compound **15d:** 3122 (υO-H), 3023 (υN-H), 2954(υN-H), 1600 (υC-N), 1512(υC-N), 1369 (υC=S), 1010 (υC-O).

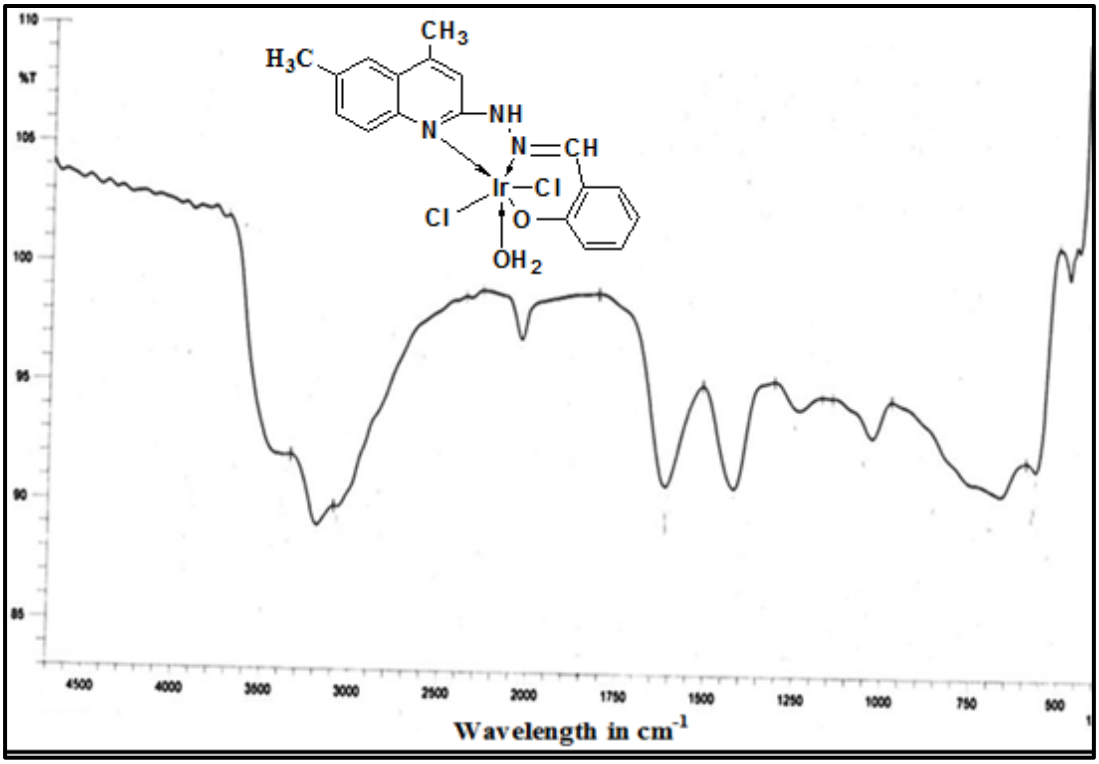

Fig 75- IR spectrum of iridium (III) complex 14b

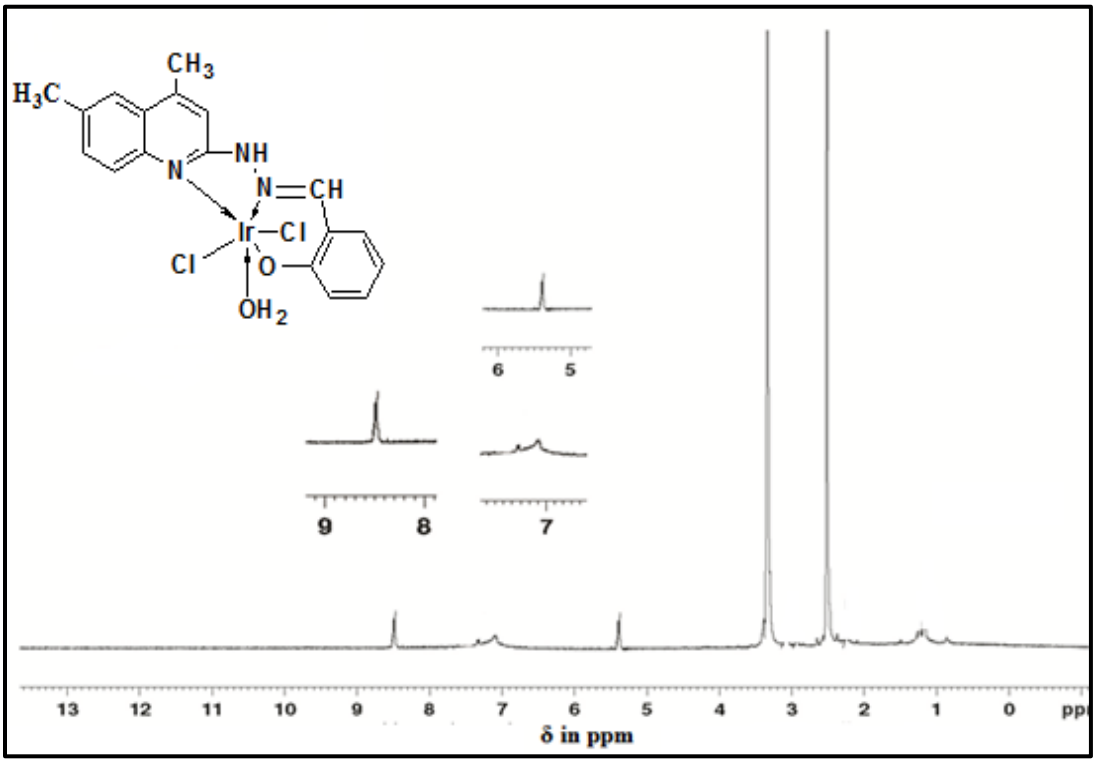

Fig 76 - ^{1}H-NMR spectrum of iridium (III) complex 14b

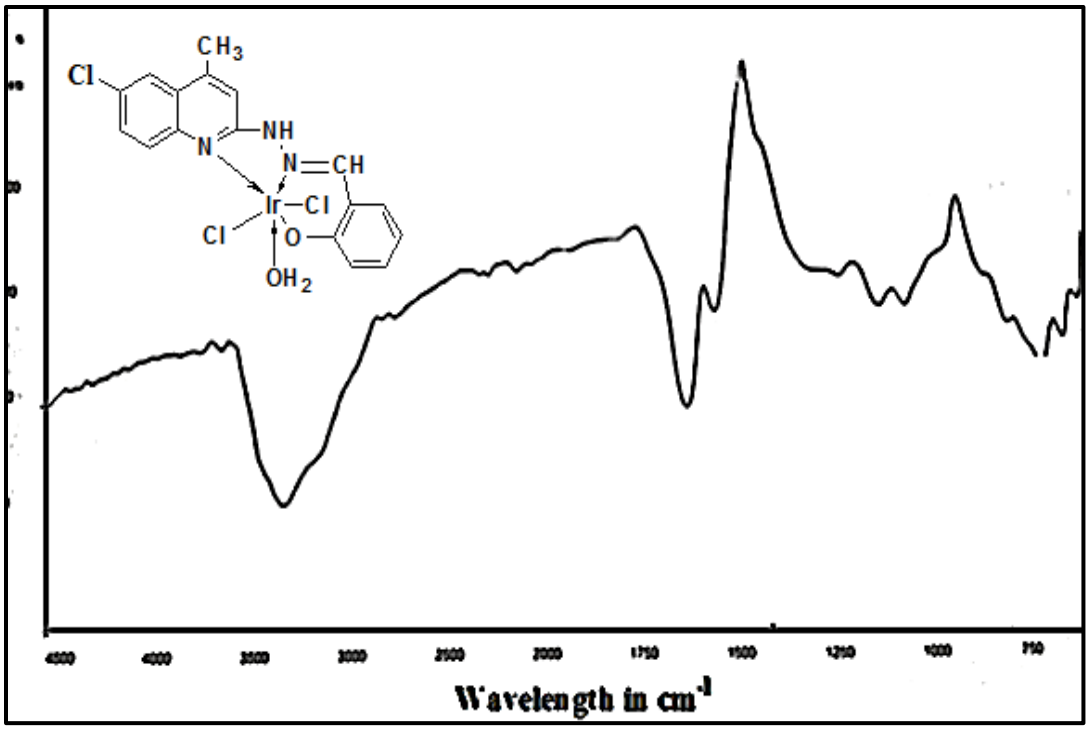

Fig 77- IR spectrum of iridium (III) complex 14c

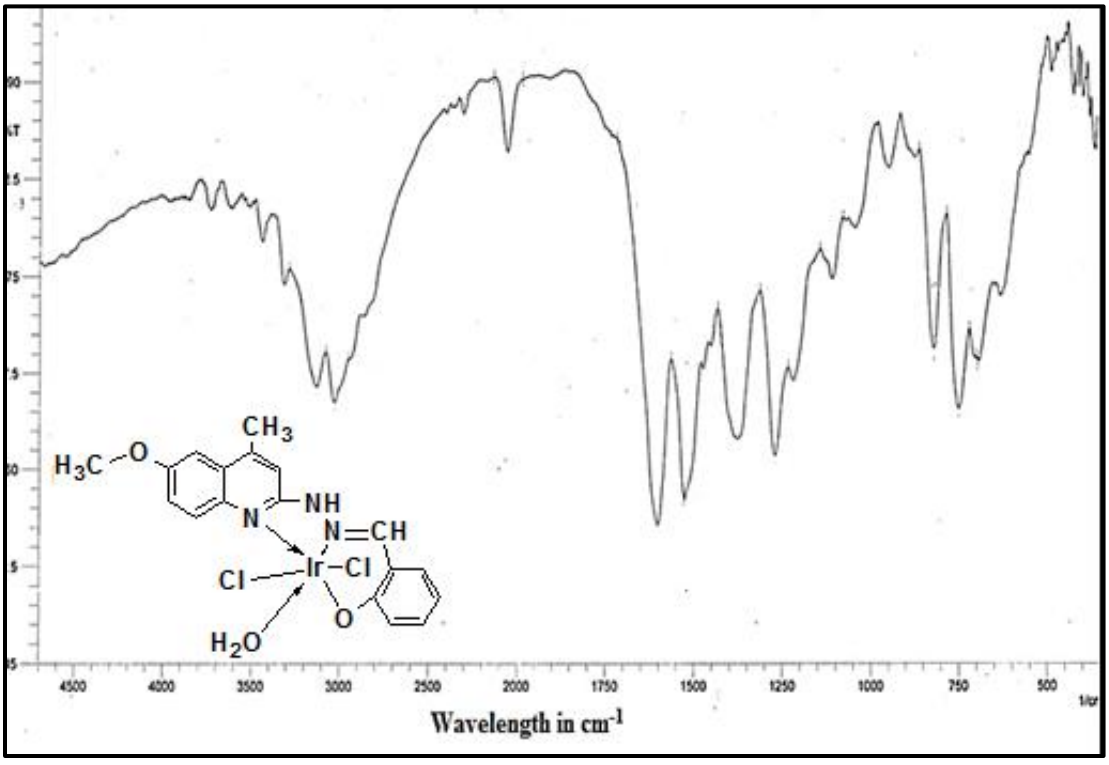

Fig 78- IR spectrum of iridium (III) complex 14d

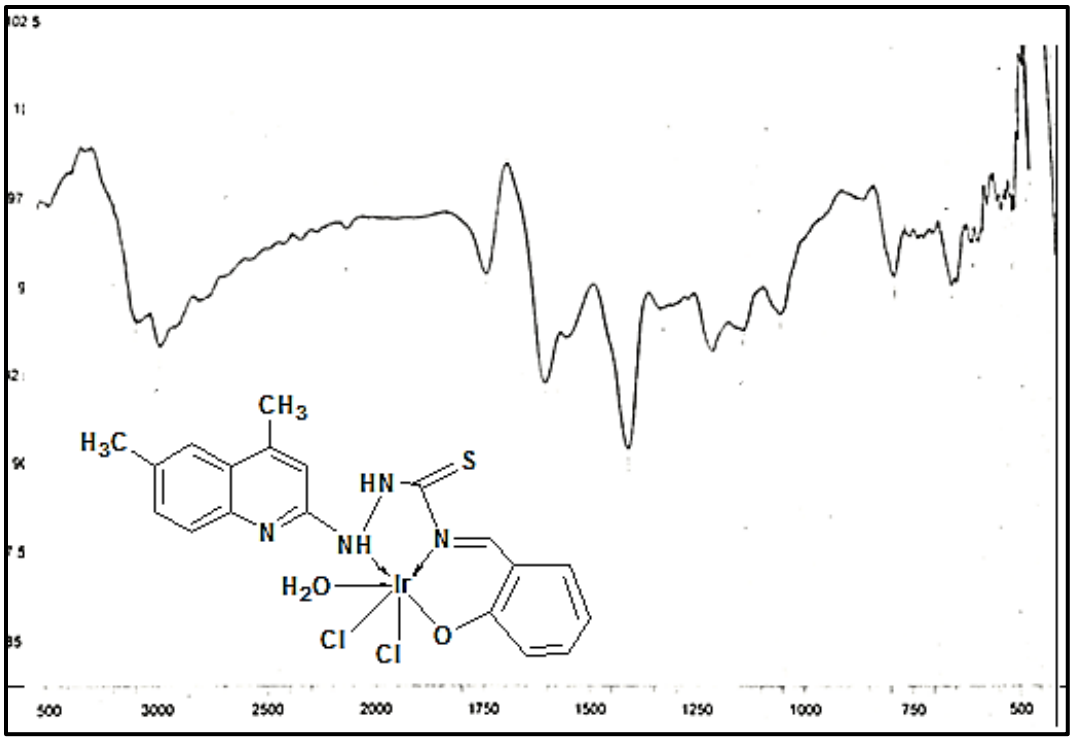

Fig 79- IR spectrum of iridium (III) complex 15b

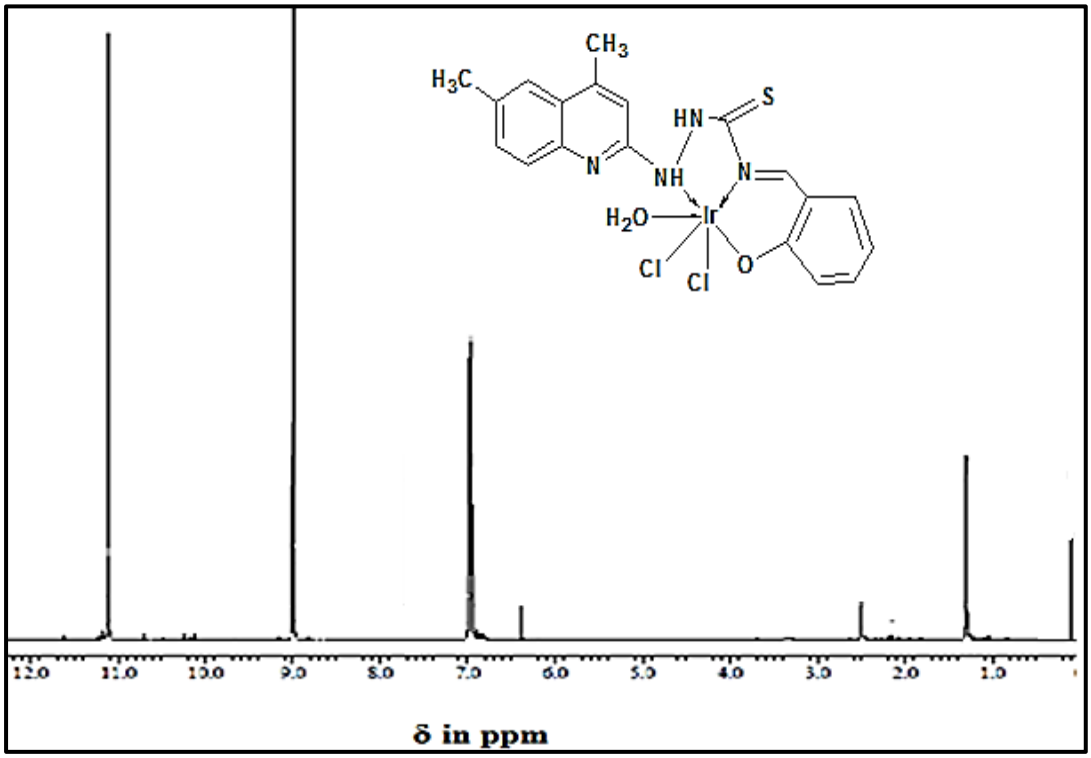

Fig 80- ^{1}H-NMR spectrum of iridium (III) complex 15b

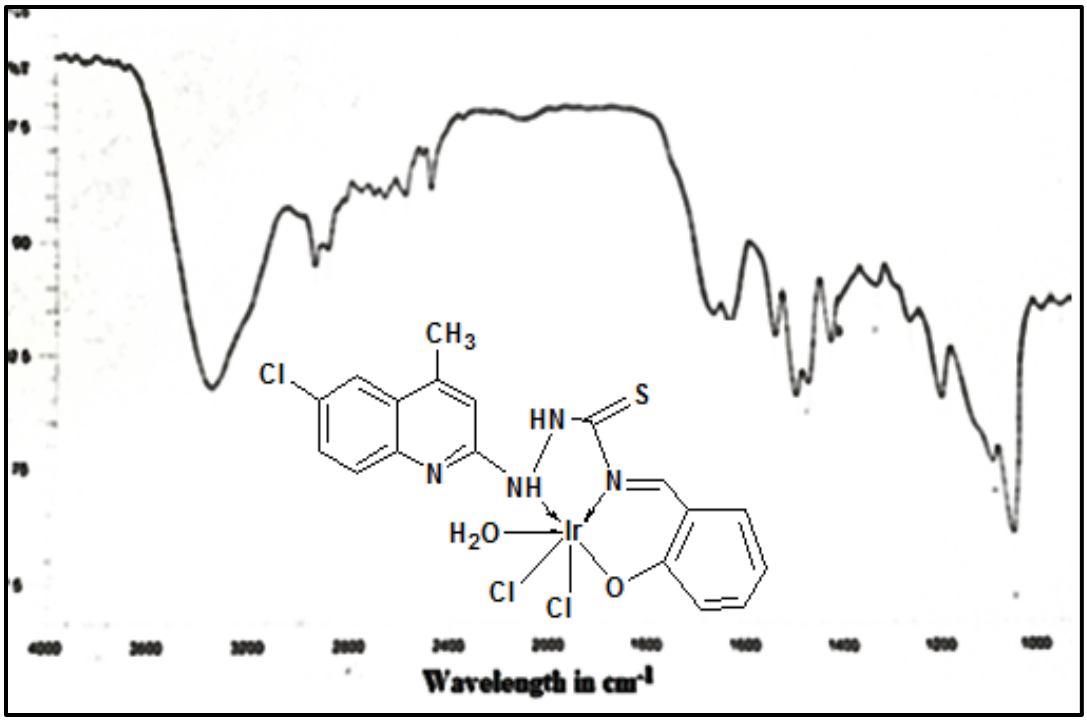

Fig 81- IR spectrum of iridium (III) complex 15c

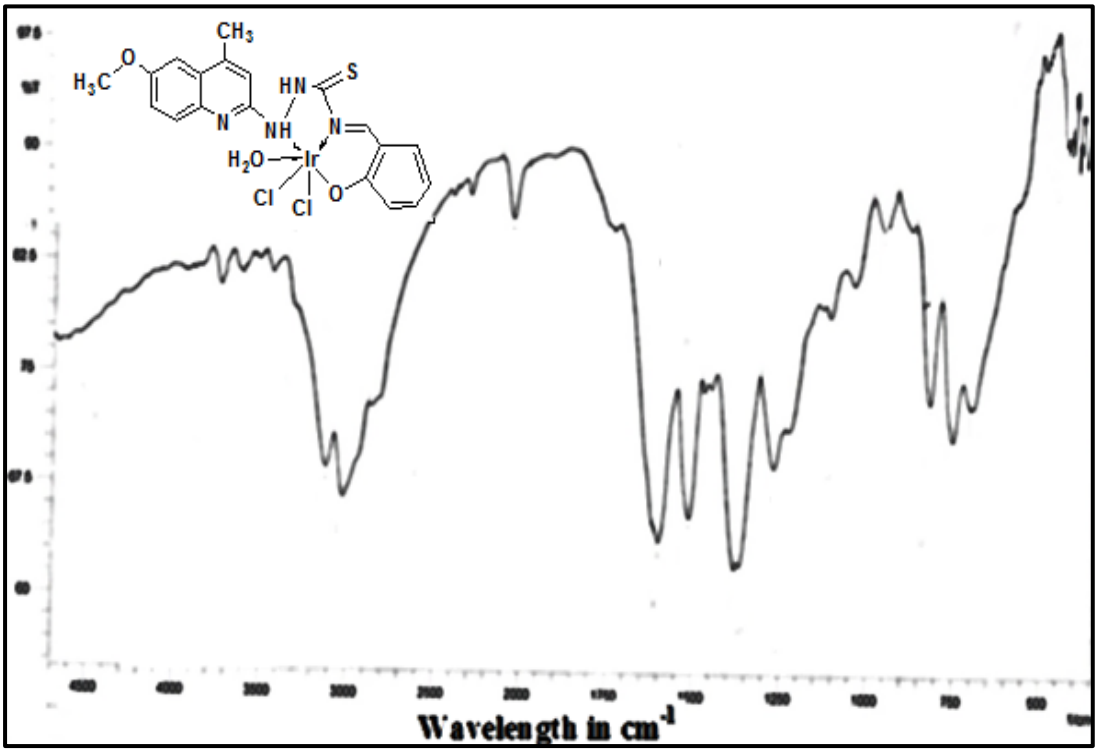

Fig 82- IR spectrum of iridium (III) complex 15d

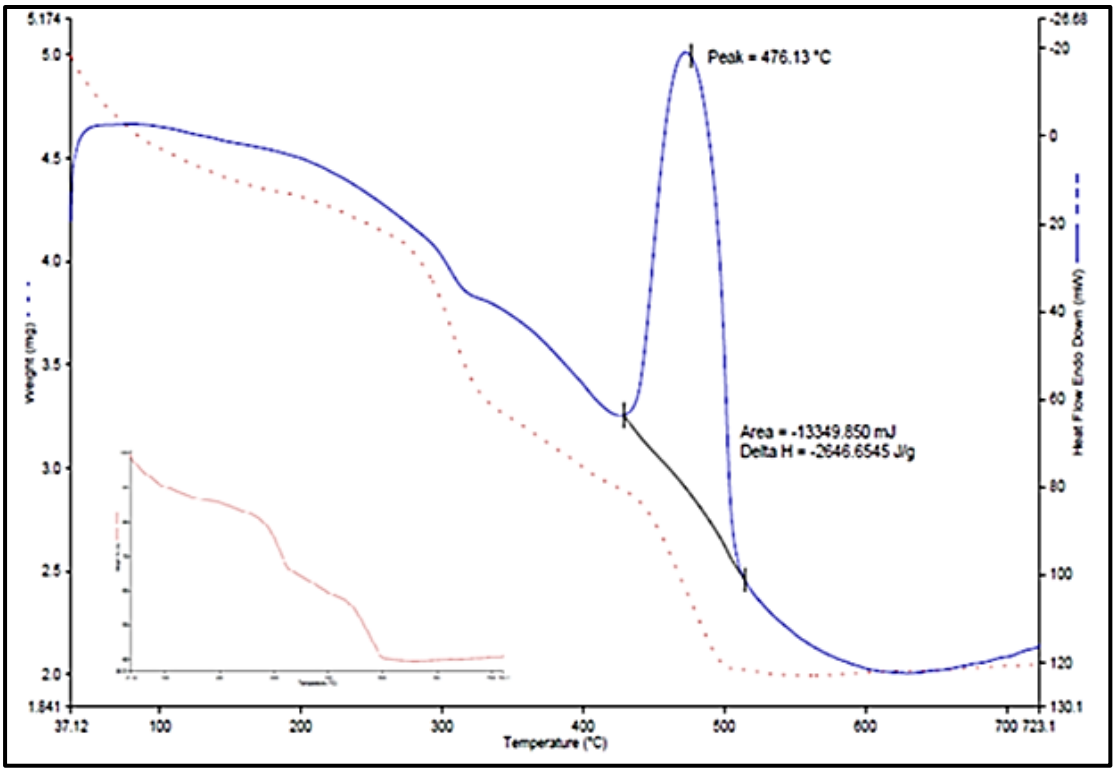

Fig 83 - TGA curve of complex 14b

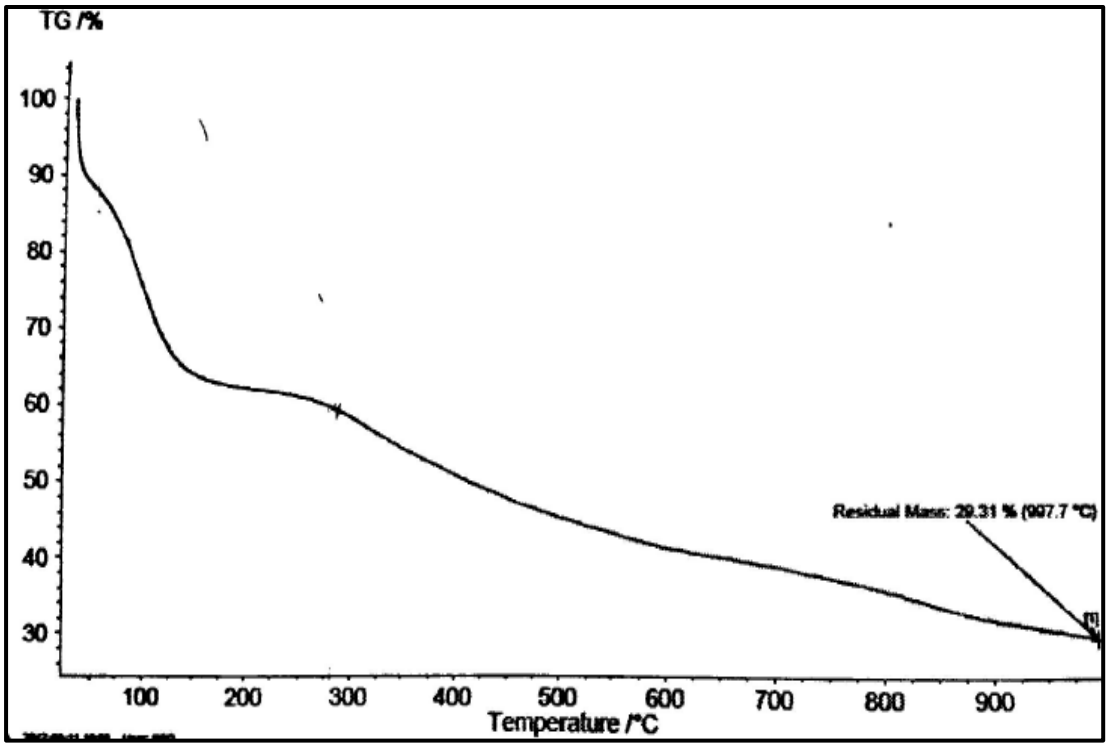

Fig 84- TGA curve of complex 15b

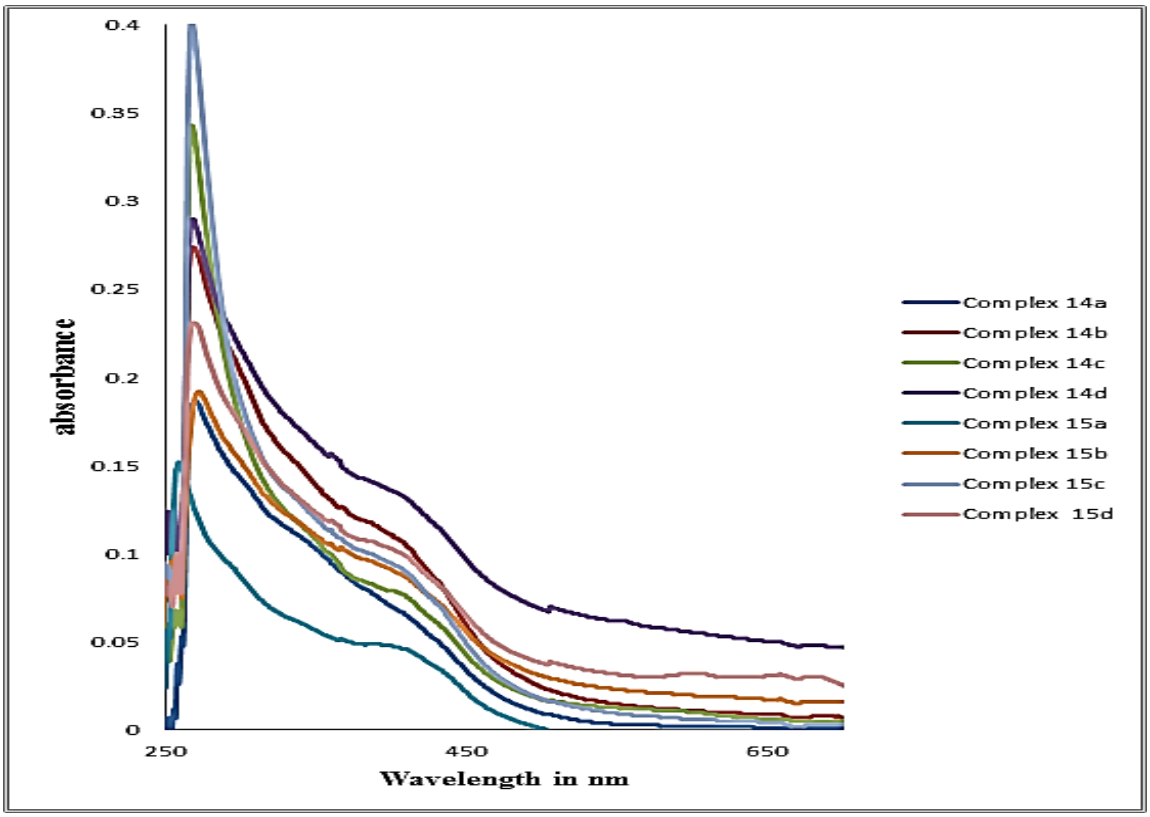

Fig 84a - UV spectrum of Ir(III) complexex 14(a-d) & (15a-d)

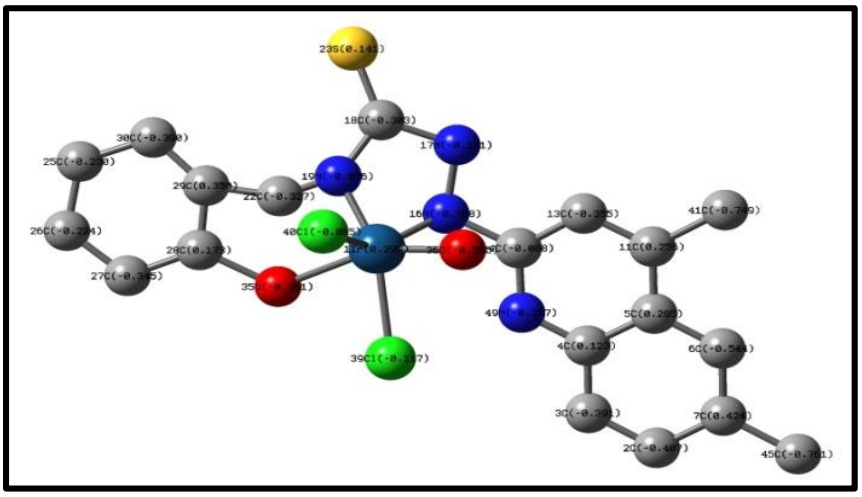

Fig 88 - Optimised geometry of iridium complex 15b

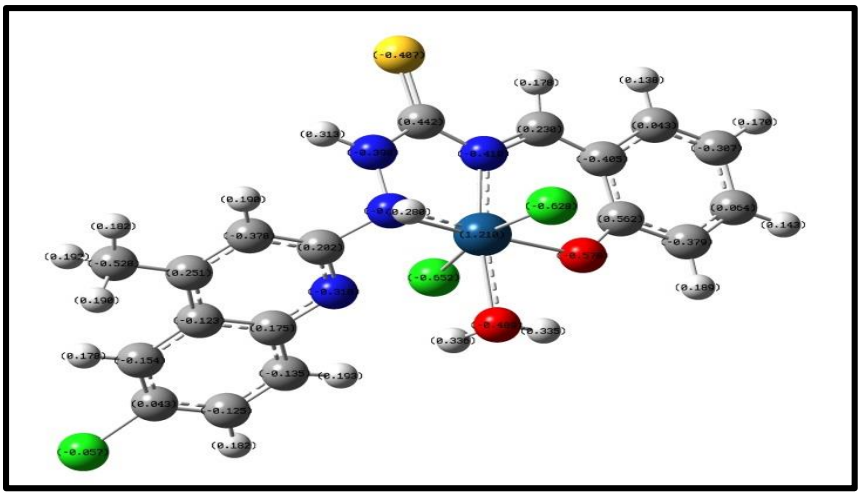

Fig 89 - Optimised geometry of iridium complex 15c

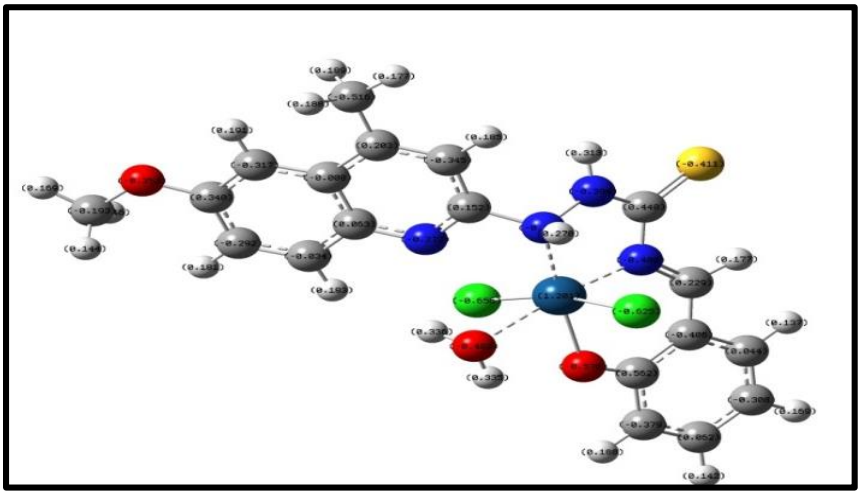

Fig 90 - Optimised geometry of iridium complex 15d

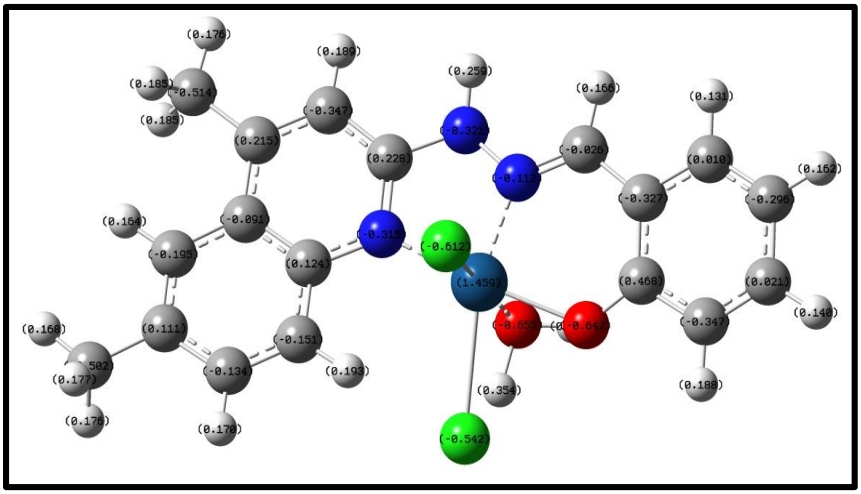

Fig 85 - Optimised geometry of iridium complex 14b

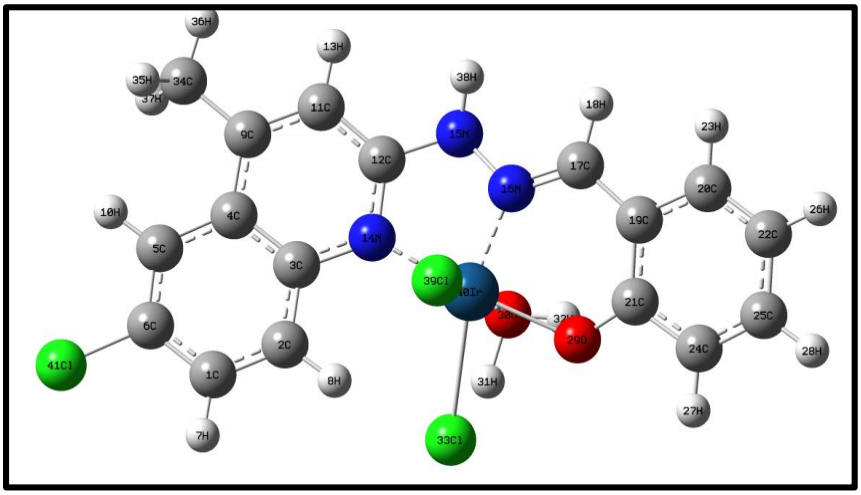

Fig 86 - Optimised geometry of iridium complex 14c

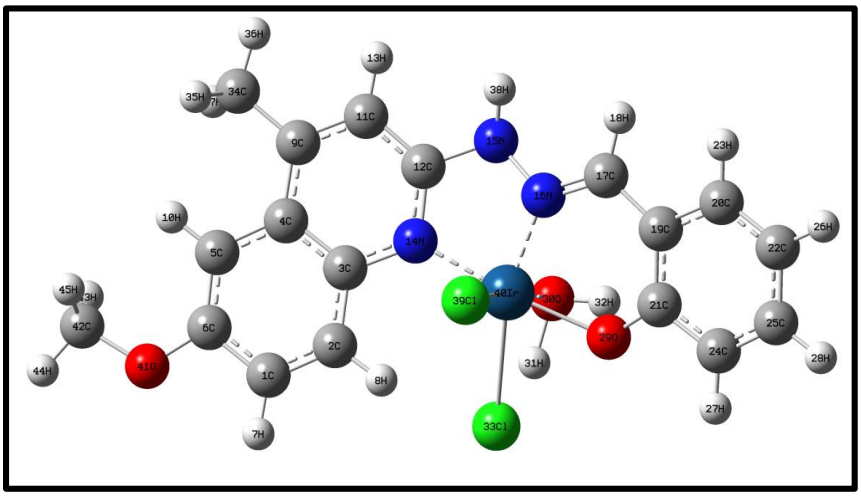

Fig 87 - Optimised geometry of iridium complex 14d

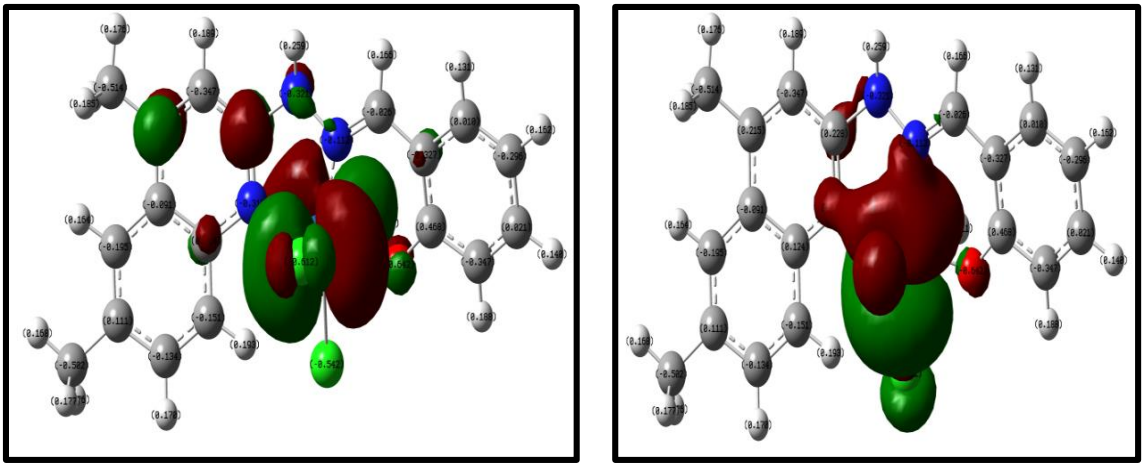

Fig 91 - Frontier molecular orbitals of iridium complex 14b

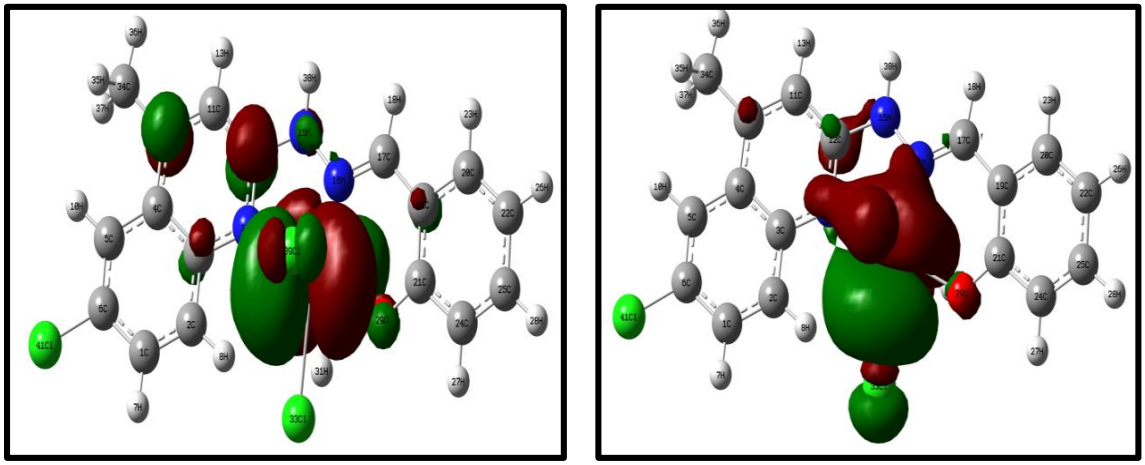

Fig 92 - Frontier molecular orbitals of iridium complex 14c

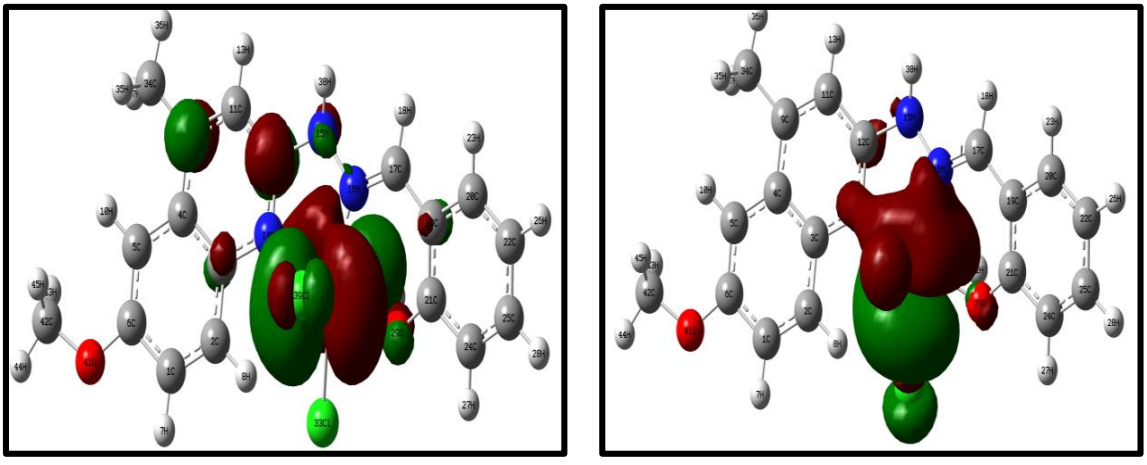

Fig 93 - Frontier molecular orbitals of iridium complex of 14d

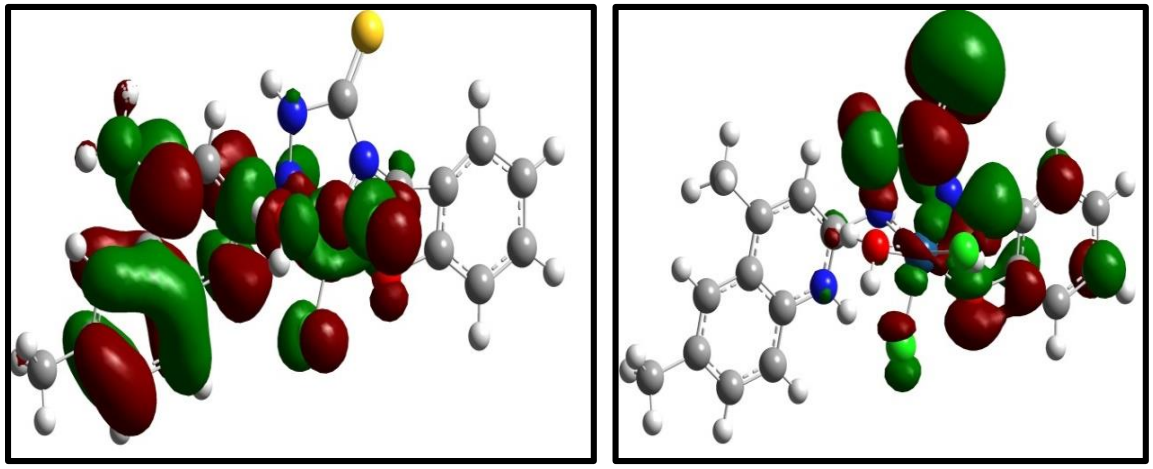

Fig 94 - Frontier molecular orbitals of iridium complex 14b

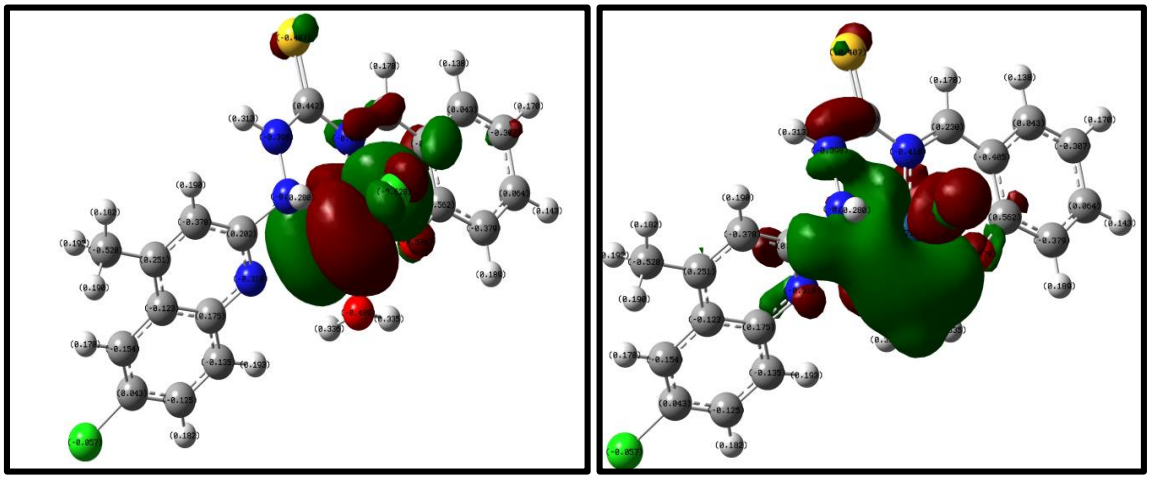

Fig 95 - Frontier molecular orbitals of iridium complex 15c

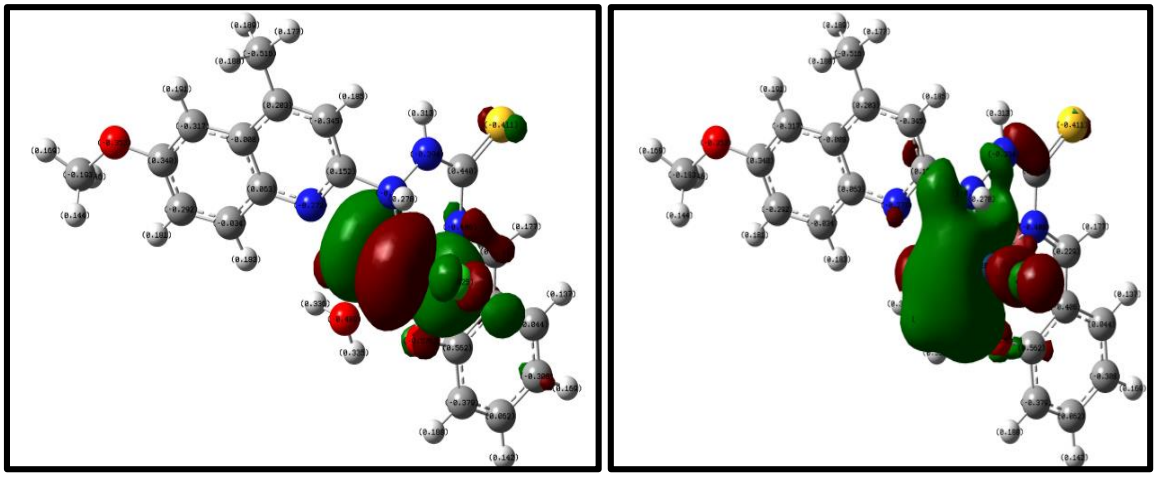

Fig 96 - Frontier molecular orbitals of iridium complex 15d

References

1. M. J. Li, P. Jiao, W. He, C. Yi, C. W. Li, Eur. *J. Inorg. Chem*, 197–200 (2011).
2. T. Hajra, S. Ghosh, J. K Bera, V. Chandrasekhar, Indian *J. of Chemistry***, 50,** 1290–1297 (2011).
3. V. Sivakumar, *Int. J. Lumin. App*, **3,** 45–48 (2013).
4. G. Zhang, H. Zhang, Y. Gao, R. Tao, L. Xin, *Organometallics*, **33,** 61−68 (2014).
5. C. Zhou, Y. Shi, X. Ding, M. Li, J. Luo, *Anal*, *Chem*, **85,** 1171−1176 (2013).
6. S Mandal, D. K Poria, D. K Seth, P Sarothi, P Gupta, *Polyhedron,* **73,** 12–21 (2014).
7. S. Mandal, R. Das, P. Gupta, B. Mukhopadhyay, *Tetrahedron Lett.,* **53,** 3915–3918 (2012).
8. L. C. Sudding, R. Payne, P. Govender, *J. Organomet. Chem.* **774,** 79–85, (2014).
9. S. I Bezzubov, V. D. Dolzhenko, Y. M. Kiselev, Russian Journal of Inorganic Chemistry, **59,** 749–755, (2014).
10. S. Mandal, D. K. Poria, R. Ghosh, P. S. Ray, P. Gupta, *Dalt. Trans,* **43(46),** 17463-17474, (2014).
11. S. K. Seth, S. Mandal, P. Purkayastha, P. Gupta, *Polyhedron*, **95,** 14–23, (2015).
12. A. Nakagawa, Y. Hisamatsu, S. Moromizato, M. Kohno, S. Aoki, *Inorg. Chem,* 53, 409-422**,** (2014).
13. J. Jayabharathi, V. Thanikachalam, R. Sathishkumar, *New J. Chem*, **39,** 235–245, (2015).
14. N. R. Palepu, J. R. Premkumar, A. K. Verma, K. Bhattacharjee, *Arab. J. Chem* (2015).doi-10.1016/j.arabjc.2015.10.011.
15. S. Sinha, S. Mandal, P. Gupta, *RSC Adv*, **5,** 99529–99539 (2015).
16. L. Lu, L. J. Liu, W. C. Chao, H. J. Zhong, M. Wang, *Scientific reports,* 1–9, (2015).
17. S. Mukhopadhyay, R. K. Gupta, R. P. Paitandi, N. K. Rana, G. Sharma, *Organometallics,* **34(18),** 4491-4506 (2015).

18. K. S. Bejoymohandas, A. Kumar, S. Varughese, E. Varathan, V. Subramaniand and M. L. P. Reddy **,** *J. Mater. Chem. C*, **3**, 7405 (2015).

19. M. L. P Reddy, K. S. Bejoymohandas, *J. of Photochem. Photobiol. C Photochem*, **29,** 29–47, (2016).

20. S. K. Seth, S. Mandal, K. Srikanth, P. Purkayastha, P. Gupta, *Eur, J. Inorg. Chem*, **2017**, *873-880 (*2016).

21. M. A. Esteruelas, A. M Lopez, E. Onate, *Organometallics***,** ***36*** **(3),** 699–707 (2017).

22. A. Kumar, R. Kumar, R. Prasad, D. Shankar, *J. Organomet. Chem*, **801,** 68–79, (2016).

23. M. V. Werrett, S. Muzzioli, P. J. Wright, A. Palazzi, P. Raiteri, S. Zacchini, M. Massi, *Inorg. Chem*, **53**, 229−243, (2014).

24. Q. Zhao, Y. Zhou, Y. Li, W. Gu, Q. Zhang, J. Liu, *Anal. Chem 2016,* **88 (3),** 1892–1899 (2016).

25. M. A. Esteruelas, E. Onate, A. U. Palacios, *Organometallis,* **36,** 1743–1755, (2017).

26. Shrabanti Das, Sourav Kanti Seth, Parna Gupta and Pradipta Purkayastha, *J. Lumin.***192**, 1196-1202 (2017).

27. Y. Zhou, K. Xie, R. leng, L. Kong, C. Liu, *Dalt. Trans,***46(2),** 355-363 (2016).

28. M. Ouyang, L. Zeng, K. Qiu, Yu Chen, L. Ji, H. Chao *Eur. J. Inorg. Chemistry*, 1764–1771 (2017).

29. C. Li, J. Lin, Y. Guo, S. Zhang, *Chem. Commun*, **47**, 4442–4444, (2011).

30. M. Wang, K. H. Leung, S. Lin, D. S. H. Chan, *Scientific Reports*, **4 ,** 6794 (2014).

31. X. Chen, H. Wang, J. Li, W. Hu, M.J. Li, *Spectrochimica Acta Part A: Molecular and Biomolecular Spectroscopy,* **173,** 904–909, (2017).

32. E. Ekengard, K. Kumar, T. Fogeron, C. Kock, P. J. Smith, *Dalton Trans*, **45**, 3905, (2016).

33. J. L. Liao, P. Rajakannu, P. Gnanasekaran, S. R. Tsai, *adv. optical matter*, 6(11) (2018) . doi-10.1002/adom.201800083.

34. S. Adhikari , O. Hussain , R. M. Phillips , M. R. Kollipara, *J. of Organometallic Chem*, **854,** 27-37 (2018).

35. C. M. D. Rosa, J. D. Hodgson, R. J. Crutchley, *J. Am. Chem. Soc*, **126 (24),** 7619–7626 (2004).

36. Z. Liu, Z. Bian, C. Huang, *organometallic chemistry* , **28**, 113-142, (2009).

37. J. Lewis, B. N. Figgis, Prog, *Inorg. Chem*, **6,** 105 (1964).

38. H. Yang, G. Meng, Y. Zhou, H. Tang , J. Zhao, Materials, **8**, 6105-6116 (2015).

39. Md. K. Nazeeruddin, R. H. Baker, D. Berner, S. Rivier, *J. Am. Chem. Soc,* **125,** 8790-8797 (2003).

40. A. Boultif, D. Louer, J. Appl. Crystallogr**, 37,** 724 (2004).